Eberhard-Karls-Universität Tübingen
Mathematisch-Naturwissenschaftliche Fakultät
Geographisches Institut

Wissenschaftliche Arbeit für die Erste Staatsprüfung
für das Lehramt an Gymnasien
Betreuer: Akad. Oberrat Dr. Joachim Eberle

Monitoring snowmelt at high temporal and spatial resolution:

a method using standard digital camera images

Leo Sold
Geographie, Mathematik
Salzstadelgasse 8, 72070 Tübingen
Email: sold.leo@googlemail.com

17. Dezember 2010

Ich erkläre, dass ich die Arbeit selbstständig angefertigt und nur die angegebenen Hilfsmittel benutzt habe. Alle Stellen, die dem Wortlaut oder dem Sinn nach anderen Werken, gegebenenfalls auch elektronischen Medien, entnommen sind, sind von mir durch Angabe der Quelle als Entlehnung kenntlich gemacht. Entlehnungen aus dem Internet sind durch Ausdruck belegt.

Leo Sold, 17. Dezember 2010

Abstract

The duration of snow cover and its hydrological and physical characteristics are crucial to High Arctic ecosystems. In this work terrestrial images taken via a standard digital camera are used to obtain information on the spatial and temporal variability of snow cover depletion in spring 2008. The research area Linnédalen is situated on about 78° northern latitude in western Spitsbergen, Svalbard. With respect to the relevant weather conditions and measurements on the snowpack the decline in snow covered area is analysed on a daily basis. The scope of this work is to contribute to a comprehensive image of the factors and processes controlling the timing and character of snowmelt in the High Arctic. The strong linkage of snow cover to climatic conditions is particularly interesting in the context of global Climate Change. On the one side, changes in seasonal snow cover will directly affect the High Arctic ecosystem and on the other side the related change in surface albedo drives one of the most important feedback mechanisms in climate change.

Zusammenfassung

Die Dauer der Schneebedeckung sowie ihre hydrologischen und physikalischen Eigenschaften sind für arktische Ökosysteme von herausragender Bedeutung. In der vorliegenden Arbeit werden aus terrestrischen Aufnahmen einer Digitalkamera Informationen über die räumliche und zeitliche Variabilität der Schneeschmelze im Frühjahr 2008 gewonnen. Das Untersuchungsgebiet Linnédalen liegt auf etwa 78° nördlicher Breite in Westspitzbergen. Unter Berücksichtigung relevanter Wetterdaten und Messungen an der Schneedecke wird die Veränderung der Schneebedeckung auf täglicher Basis ausgewertet. Ziel der Arbeit ist es, zu einem umfangreichen Verständnis der Faktoren und Prozesse beizutragen, die den Zeitpunkt und Ablauf der Schneeschmelze unter hocharktischen Bedingungen bestimmen. Die starke Abhängigkeit der Schneedecke von den klimatischen Gegebenheiten ist besonders in Hinblick auf eine zukünftige Änderung des Klimas interessant. Veränderungen wirken sich zum einen unmittelbar auf das Ökosystem aus und sind über die hohe Albedo der Schneedecke gleichzeitig zentraler Bestandteil des wohl wichtigsten Feedback-Mechanismus im Rahmen des Klimawandels.

Contents

List of Figures

List of Tables

1 Introduction

The presence of water is one of the most important factors for all kinds of biological activity. Mankind as well as flora and fauna directly depend on its availability that varies widely in different ecosystems. At the same time water distribution varies both spatially and temporally. In high latitudes, snow is the most common form of precipitation and a large part of the annual precipitation is stored as either snow or ice during winter. When it melts in spring, it is rapidly released as meltwater runoff. This leads to peak river discharge and water levels, and makes up the most influential hydrological input in these ecosystems. Furthermore, the duration of absent snow cover during summer marks the time of thawing in the upper parts of the permafrost, the active layer. Such thawing of the active layer makes the soil susceptible to transportation and denudation.

The presence of snow cover, and the circumstances that lead to melting, are an important area of current climate change research. Indeed, the IPCC Assessment Report notes:

> *"Snow, ice and vegetation play vital roles in the global climate system, through albedo and insulation effects. Since the [IPCC Third Assessment Report in 2001], increasing evidence has emerged indicating a more rapid disappearance of snow and sea-ice cover in some areas [...], and consequent changes of albedo may be leading to further climate change [...]."* (Anisimov et al. 2007: 661)

This double sided importance to ecosystems makes snow an exceptionally interesting subject of research: on the one side snow and its melting are essential to various processes on the local scale and on the other side snow cover drives major feedbacks on global climate change. This thesis therefore aims to contribute to a comprehensive understanding of the processes and factors controlling the spring melt of snow cover. It is based on a time series of snow cover data in Linnédalen, western Spitsbergen (Svalbard, Norway), covering spring 2008. Information about the depletion of snow cover is obtained by analysing pictures taken via a time-lapse camera with adequate methods to gain data about the percentage of snow covered area. The snow cover data is compared with weather information as well as information from temperature sensors within the snowpack. For calibration, additional data about the snowpack was taken in the field in early summer 2008. The research area on Svalbard benefits the analysis procedure due to an undisturbed melting and a precisely definable spring-term.

To establish a better understanding of processes taking place during springmelt, this work's first chapter gives a summary of the respective knowledge and theory. It focuses on the relevant

factors controlling the melting of snow, including a range of meteorological and terrestrial processes. Afterwards, the methods used to quantify those processes are outlined. Here, special emphasis is given on the analysis of the time-lapse camera pictures, which is performed using a greyscale threshold to distinguish snow from bare ground. Meteorological data is derived from a small weather station placed in the research area that is enhanced by a set of temperature sensors within the snowpack. Together with the measurements taken for calibration during fieldwork the results are presented in the according chapter. The time-series is analysed with respect to different phases of the melting period and spatial differences within the area of interest. Difficulties and problems regarding the analysis procedure call for a detailed discussion, which also includes possible improvements to the method in the context of similar studies. The thesis closes with a reflection of processes that make snow cover exceptionally vulnerable to a changing climate.

The importance of snow cover especially for mountainous regions and in high latitudes is subject of intensive present-day research. There are a number of studies that use similar methods to achieve spatial and temporal information on the spring depletion of snow cover. Schmidt (2007) puts special emphasis on the relation of snow cover depletion and topography in the alpine Lötschental, Switzerland. Long term monitoring of snow covered area and its effect on vegetation is carried out in the Zackenberg Research Area in northwest Greenland by Hinkler et al. (2002, 2003) while Christiansen (2004) puts special emphasis on the relation to the thawing of frozen ground. Their work contributes important information to this thesis and their results are thoroughly taken into account.

2 Research area

The Svalbard archipelago is situated about 650 km north of the Norwegian mainland in the Barents Sea. It extends from 74° to 81° latitude with an approximate land mass of 61 020 km^2 total land area (Bore et al. 2009: 4). National parks or other types of protected areas make up 65% of the area which is slightly more than the 60% covered by glaciers (Bore et al. 2009: 4). Ground that is not covered by glacial ice is permafrost which can extend to more than 100 m depth depending on local topographic constraints (Humlum et al. 2006). Svalbard's largest island is Spitsbergen in the southwest of the archipelago, which is also the setting for the research presented in this work.

Linnédalen is situated near Kapp Linné, the northwestern end of the Spitsbergen peninsula. With an elevation close to sea level, the U-shaped valley is oriented in south-north direction on about 78° latitude at the southern side of the Isfjord inlet (figure 1). It is about 10 km long and 2 km wide while Griegfjellet (781 m a.s.l.) marks the highest elevation of the surrounding topography.

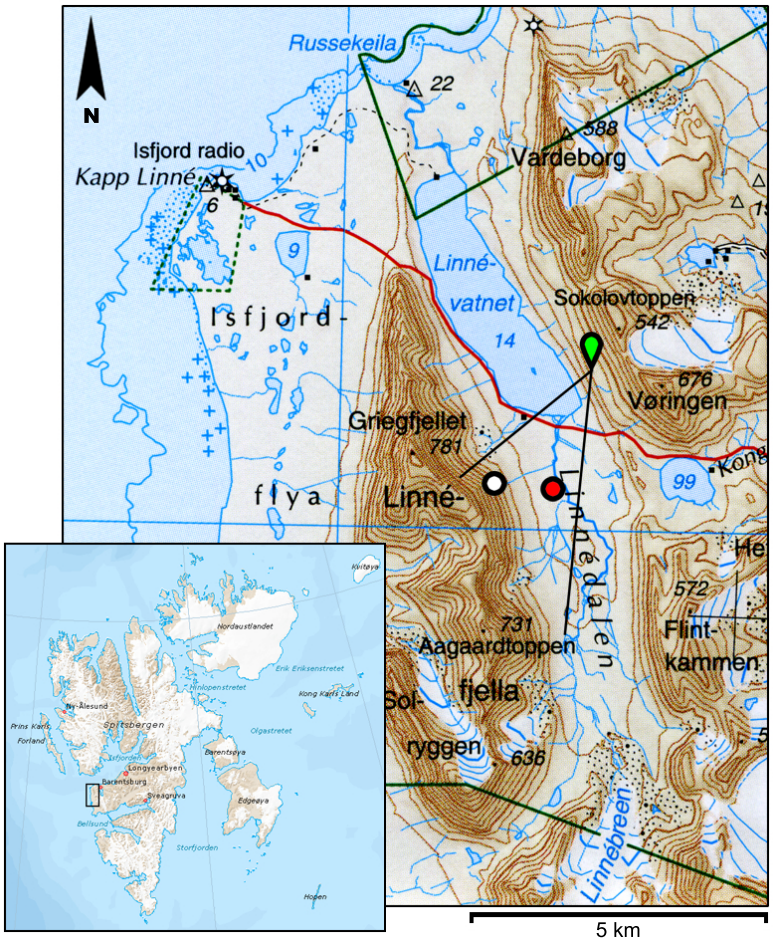

Figure 1: Map of the research area Linnédalen, Svalbard. The green pin represents the position of the digital camera with the angle of its view marked in black; the red pin represents the weather station position; the white pin represents the investigated snow-patch. Modified according to Norsk Polarinstitutt (2008). Archipelago overview map: Norsk Polarinstitutt (2010).

Linnébreen makes up its southern end and associated meltwater feeds a glaciofluvial-lacustrine system consisting of Linnéelva (creek) and Linnévatnet (lake). The latter is situated at the north end of the valley. As emphasis for the active permafrost, sorted circles, ice-wedge polygons and solifluction features can be found in the valley as well as rock glaciers on the upper valley slopes.

The high latitude of the study site results in an Arctic climate (figure 2). Monthly average temperatures from Isfjord Radio, a former radio station at Kapp Linné and in close proximity to the study site, vary from -12.4°C in February to 4.8°C in July and are highly affected by the annual cycle of radiation intensity. The polar night lasts from mid November to the end of January and the polar day from mid April to late August respectively (Bore et al. 2009: 4). The location on the

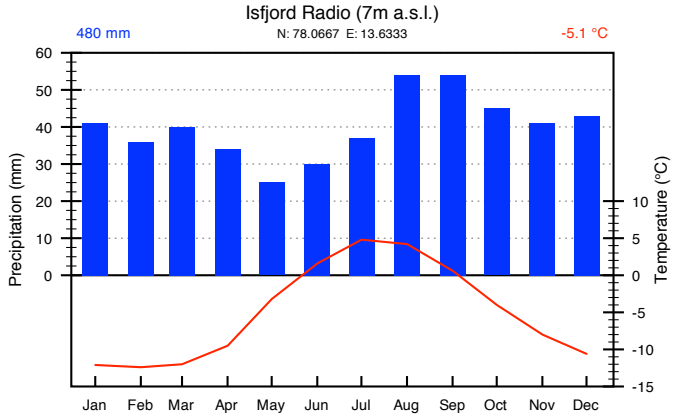

Figure 2: Climograph illustrating temperature and precipitation data from Isfjord Radio, Svalbard. Data represents average monthly values between 1961–1990. Data source: Norwegian Meteorological Institute (2010).

western coast of Svalbard results in slightly higher annual average temperatures of -5.1°C compared to more centralised localities on Svalbard, than for example Longyearbyen, which shows an annual average of -6.0°C (Norwegian Meteorological Institute 2010).

Annual precipitation is about 480 mm, which is rather low but much higher than it is further inland. This mirrors the remnants of the North Atlantic Current influencing the climate of southern and western Svalbard and making Svalbard's climate generally milder than it is for instance on the same latitude in Canada (e.g. Bore et al. 2009: 5). In the context of this investigation, precipitation values have to be carefully considered as snow is known to be redistributed by wind (see chapter 4 or e.g. Dingman 2002: 169f). Naturally, precipitation plays a major role in this work, with emphasis on snow as the solid type. The chapter on theoretical background will deal with precipitation types and snow cover as well as their characteristics in the High Arctic in greater detail.

3 Theoretical background

3.1 Snow cover characteristics

Snow is a complex medium that consists of ice, pore spaces and – if temperature allows – of free water (Dingman 2002: 166). Its physical, mechanical and optical properties vary widely with the proportion of the three phases. The individual snowpack characteristics therefore depend not only on the formation in the atmosphere but also on terrestrial processes as it will be outlined in the next chapters.

3.1.1 Formation, distribution and redistribution of snow

Ice crystals form in the troposphere through the condensation of water vapour onto freezing nuclei when the air is supersaturated with water vapour, temperatures are low enough and freezing nuclei are available. The subsequent crystal growth is determined by further deposition of water vapour as well as the collision with supercooled water droplets that freeze onto the ice crystal (McClung & Schaerer 2006: 43f). The form of the generated crystal depends on air temperature and saturation that determine growth rates along different axes. A large ice crystal with a complex shape can then be referred to as a snow crystal (Gray & Prowse 1993: 7.2). The hexagonal symmetry of snow crystals originates from the molecular structure of water. A comprehensive outline of involved processes and crystal forming is given by McClung & Schaerer (2006). Once the crystal is too heavy to be kept in suspension it starts falling as precipitation while further crystal growth, forming or melting depend on the vertical atmospheric temperature profile. While falling, snow crystals aggregate into snowflakes (Gray & Prowse 1993: 7.2).

The fraction of precipitation falling as snow is naturally high in polar regions. Førland & Hanssen-Bauer (2000: 488f) present measurements from Ny-Ålesund, Svalbard for 1975–1996 with 25% of total precipitation (403 mm) falling as rain, 44% as snow and 31% as mixed type which is mainly sleet. Only from June to September, monthly rain values exceed the ones of snow. The spatial distribution of snowfall in the research area follows the distribution of total precipitation as outlined in chapter 2. Here, the orographic situation and increasingly continental climate further inland play the main roles, while on the local scale the interaction of wind and topography determine the accumulation of newly fallen snow. Distribution and redistribution of snow by wind are subject of many hydrological modelling efforts, since they largely determine local snow water equivalent (e.g. Pomeroy et al. 1997). Blowing snow is transported by either saltation or suspension, while creep or rolling is of little relevance (Gray & Prowse 1993: 7.2). Saltation takes place in the lowermost couple of centimeters above the snow surface where snow crystals skip over the snow on the ground. Once snow crystals are eroded by wind saltation begins and makes them susceptible for suspension. Suspension is the transportation of snow by atmospheric turbulence within several tens of metres above the snow surface (Pomeroy et al. 1997: 1452). The two processes change the proportions of the total blown snow when wind speed changes: saltation generally contributes less than 25% while with increasing wind speed the amount of suspended snow increases much faster (Pomeroy et al. 1997: 1452).

Generally, topography and vegetation determine both – sources and sinks for blowing snow by their influence on local wind speed and are therefore crucial to the development of the snow cover from new and redistributed snow (e.g. Gray & Prowse 1993: 7.5ff). Since there are neither

trees nor shrubs on Svalbard (Bore et al. 2009: 6) and the cushion plants and other short vegetation does not contribute to accumulation of blowing snow, vegetation will be neglected here. Instead the deposition of snow in lee areas, depressions and behind ridges is of major importance since the higher water equivalent means a later disappearance of snow cover. The analysis part (chapter 6) will show the actual effect of topography on the depletion of snow cover. Pohl & Marsh (2006: 1775) additionally point out that High Arctic environments show large rates in redistribution of snow because there are less melt- or rain-refreeze events in winter that stabilise the snowpack and prohibit its erosion. The relevance of blowing snow to the variability of snow distribution can be documented by the changes of local snow water equivalent which can range widely – from 50% to 400% in proportion to local measured snowfall, according to Pohl & Marsh (2006: 1776).

The aeolian transportation of snow also influences the structure of the snowpack. The mechanical friction brakes the branches of snow crystals and thereby increases the density of accumulated snow (McClung & Schaerer 2006: 32). The physical characteristics of the snowpack are illustrated in the next chapter.

3.1.2 Density and the insulating character of the snowpack

The amount of precipitation stored as snowpack during the winter can be assessed as the respective water equivalent of the snow (SWE). For a given SWE, the thickness of snow cover is determined by its density, which depends on individual conditions: Ordinary, freshly fallen snow has a density in the range of 50 to 65 $\mathrm{kg\,m^{-3}}$, which can increase to 300 $\mathrm{kg\,m^{-3}}$ when the snow settles (Gray & Prowse 1993: 7.5). As stated above, winddrift increases the density of the affected snow up to 350 $\mathrm{kg\,m^{-3}}$. Further, the storage of infiltrating meltwater in the snowpack can significantly increase density in spring (Gray & Prowse 1993: 7.5).

The low density especially of fresh snow points to its high porosity which decreases with time when the snow settles. It allows a limited circulation of air in the snowpack, the movement of free water and determines the low thermal conductivity of snow and therewith its insulating character. The thermal conductivity of snow is about 0.08 to 0.42 $\mathrm{W\,m^{-1}K^{-1}}$ in dependence of its density. For ice with a density of about 900 $\mathrm{kg\,T^3}$ it is much higher with 2.1 $\mathrm{W\,m^{-1}K^{-1}}$ (Hock 2005: 366). The heat is transferred not only by conduction through the network of ice crystals but also by diffusion of air and water vapour through the pore spaces (McClung & Schaerer 2006: 38). The convection of heat in the pore spaces is documented as a particular feature of low density Arctic snow cover that has a high vertical temperature gradient and thereby supports

convection (McClung & Schaerer 2006: 38). Although the thermal conductivity depends on the snowpack properties, it is generally very low and results in its insulating character.

3.1.3 Snowpack metamorphism and stratigraphy

The increase in density when fresh snow settles already indicates that there occur not only changes in spatial distribution, but also in physical characteristics of the snow cover throughout the winter. The changes are due to variations in the form and bedding of the snow crystals. Fresh snow is made up by snow crystals in a more or less hexagonal and complex shape that build up the initial snowpack. Their form ranges from needles or prismatic to star-like shape and can be categorised by the ICSI Classification for Newly Fallen Snow Crystals (McClung & Schaerer 2006: 47–50).

Once deposited, the changes of crystal forms due to pressure, sublimation and deposition are referred to as snow metamorphism. The involved processes are particularly interesting to snow strength and stability, e.g. in avalanche work. The destructive or equal-temperature metamorphism produces rounded grains without branches through differences in the micro-scale water vapour pressure over curved surfaces (McClung & Schaerer 2006: 54). The underlying process is the vapour pressure gradient driven sublimation of water molecules at the convex and deposition at the less convex (or concave) surface. The temperature-gradient metamorphism depends on a strong temperature gradient between the snowpack bottom and the surface. This also results in water vapour pressure differences and hence, transportation of water molecules along this gradient from bottom to top. The deposition takes place in the upper snowpack and builds up facets on the snow grains. A detailed outline of snow metamorphism is given e.g. by (McClung & Schaerer 2006). Although these processes do not affect the SWE, they still change some relevant characteristics of the snowpack such as density (Gray & Prowse 1993: 7.5) and optical properties. Increased snow grain size in the upper snowpack decreases albedo and promotes a deeper penetration of shortwave radiation, which in turn influences the temperature within the snowpack and therewith metamorphism (Gerland et al. 1999: 2337–2341).

3.2 Energy balance and the melting of snow

3.2.1 Phases of the melt period

The melt period starts when the snowpack's net energy input is constant positive (Dingman 2002: 185). From the hydrological aspect, this period can be separated into three phases (see Dingman 2002: 185–190), which will later be used to structure the analysis part:

- *The warming phase:* Before any melting of the snowpack can occur, its temperature has to be at the melting-point of 0°C. The cold content, which is the lack of energy that is necessary to warm up the snowpack until it is isothermal on 0°C, has to be removed. The warming phase does not necessarily start with air temperatures above 0°C, but at the point where temperatures within the snowpack start to increase.
- *The ripening phase:* Analogous to the field capacity of soil, snow can retain a certain amount of water in the pore spaces between snow grains. As soon as melting occurs, pores start to get filled with meltwater, which is kept in the snowpack by surface-tension forces.
- *The output phase:* When the holding-capacity for liquid water is reached ("ripe"), the snowpack cannot retain more meltwater in the pore spaces. Any further energy input now produces water output.

It should be noted here, that some melting can occur in the warming period in the upper snowpack due to the low thermal conductivity on snow (chapter 3.1.2). Meltwater then percolates into the snowpack reaching temperatures below 0°C. This forces the water to refreeze and release latent heat which again contributes to the warming of the snowpack (French 2007: 239).

3.2.2 Modelling snowmelt

Today's research offers a couple of ways how to model snowmelt. They are based on different approaches of how to estimate the energy available for melting and vary a lot in accuracy but also complexity. The idea of this work is not to model snowmelt, but to get an idea about which factors contribute to melting. Snowmelt models require quantification of the relevant processes and are therefore brought up here.

The Temperature-Index Approach is based on air temperature data and assumes that the daily snowmelt is a linear function of temperature. This kind of models must be calibrated by a "degree-day-factor", which is the assumed amount of melting per day and per degree. Further, they require as an air temperature-threshold for melting that is usually around 0°C (Dingman

2002: 210). This approach can give a good estimation of daily snowmelt if the degree-day-factor suits the respective local conditions (Dingman 2002: 210). Gray & Male (1981: 418) provide a way to calculate this degree-day-factor. Their formula is based on

- snow albedo, changing with time due to impurities on the snow surface
- vegetation canopy density, which can actually be neglected for the High Arctic study site
- solar radiation as an index of actually received solar radiation, reduced by slope and aspect.

The Energy-Balance Approach tries to actually quantify the energy fluxes on the snow surface with the assumption that all energy is used for melting when the surface temperature exceeds 0°C. The energy balance can be expressed as

$$Q_N + Q_H + Q_L + Q_G + Q_R + Q_M = 0 \tag{1}$$

where Q_N represents net radiation, Q_H the sensible heat flux, Q_L the latent heat flux, Q_G the ground heat flux, Q_R the sensible heat flux by rain and Q_M represents the energy used for melting (Hock 2005: 366). Sensible and latent heat fluxes represent the turbulent heat fluxes. A positive sign means a positive energy flux towards the snow surface. The energy available for melting can then be calculated using the latent heat of fusion of snow (Hock 2005: 366). Models using this physical approach require a large amount of data and are fairly complex. They are more sophisticated than the Temperature-Index models but provide precise snowmelt simulations (Dingman 2002: 210, 212).

The two main approaches can be combined to obtain the Hybrid Approach, an advanced version of the Temperature-Index, to improve the accuracy by including variables that characterise radiation. It requires less data than using the energy-balance and still gives good results (Dingman 2002: 211–214). In the context of this work, the modelling approaches show that temperature alone can not be taken as the proxy for melting. More factors need to be taken into account. The degree-day-factor in the Temperature-Index Approach already shows that radiation plays a major role for the energy budget of a snowpack. Taking a closer look to the energy-balance formula (1) helps to make out the major contributing factors. According to Hock (2005: 368f), Q_N as the net all-wave radiation can be written more precisely as

$$Q_N = (I + D_s + D_t) \cdot (1 - \alpha) + L_s^{\downarrow} + L_t^{\downarrow} + L^{\uparrow} \tag{2}$$

where on the shortwave side I represents the direct solar radiation, D_s the diffuse sky radiation and D_t the reflected radiation from surrounding terrain. Together they make up the global radiation. A part of it gets reflected from the surface, represented by the albedo α. On the longwave side $L_s^{\downarrow}$ is radiation from sky, $L_t^{\downarrow}$ from surrounding terrain and $L^{\uparrow}$ the emitted longwave radiation (Hock 2005: 368f).

3.2.3 Shortwave radiation characteristics of snow

The energy input from shortwave radiation is basically dependent on geographical location, season and time. The division into direct (I) and diffuse (D) components (formula 2) is done because parts of the solar radiation are reflected and scattered by clouds and aerosols. In mountainous regions, the reflected shortwave radiation from the surrounding terrain has to be taken into account (King et al. 2008: 74). The major influences to the amount of incoming shortwave radiation are therefore the presence of daylight, slope and aspect, the adjacent terrain and the presence of clouds. The terrain affects shortwave radiation not only by providing reflected radiation, but also by reducing direct sky radiation (Hock 2005: 369f). This is similar to the impact of clouds – they reduce direct solar radiation but increase the diffuse part. Both, terrain and clouds can produce multiple reflections (King et al. 2008: 74).

Snow albedo is studied extensively since it has a large effect on the surface radiation properties not only on the local scale but also regarding the global warming feedback mechanism (e.g. Anisimov et al. 2007: 661). Albedo is referred to as the ratio of reflected shortwave radiation to incoming global radiation on a surface. Hence, it directly controls the amount of energy input by shortwave radiation to this surface. The optical properties of snow vary a lot depending on snow wetness, impurities, grain size and properties, the surface roughness and also the properties of the incoming radiation (Gray & Prowse 1993: 7.16). Gerland et al. (1999: 2340) point out that the shortwave reflectance of snow is mainly dependent on grain size within the upper 20 cm of the snowpack and the amount of impurities (mostly soot) on the surface. Values vary from 0.95 for clean, fresh snow in early spring to 0.6 for fairly old snow in late spring. Thin or contaminated snow covers as well as the bare ground show significantly lower values. The changes in grain size and liquid water content due to snow metamorphism and melting in spring lead to an albedo decrease as it is shown in figure 3. Macroscopically invisible and visible particles may successively cover the snow surface and contribute to this effect (Gerland et al. 1999: 2340).

Thinning of the snowpack also decreases albedo when reaching a certain value of snow depth. This is because a thin snowpack gets transparent for shortwave radiation (Gerland et al. 1999: 2341;

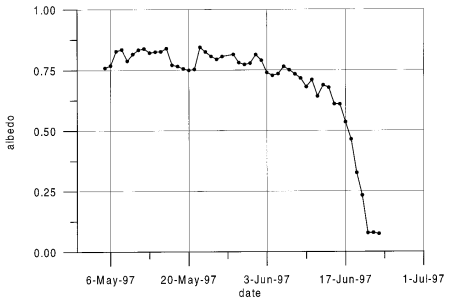

Figure 3: Snow albedo changes in Ny-Ålesund, Svalbard during spring 1997 (Gerland et al. 1999: 2339).

Winther et al. 1999: 2036f). Various values for this threshold are published – Gerland et al. (1999: 2341) suggest 20 cm. They assume that the albedo decrease together with meteorological conditions such as precipitation and clouds make up the major part of snow depth decrease when the snowpack is fairly thin. When studying the optical properties of snow on their site near Ny-Ålesung, Gerland et al. (1999: 2341) expected the change of albedo values due to different sun angles to be less than 5% and the albedo increase due to clouds to be fairly small.

3.2.4 Longwave radiation characteristics of snow

Snow is fairly sensitive to longwave radiation since it has a very low reflectance for this spectral region. With an emissivity ranging from 0.99 to 0.98 it acts as an almost perfect black body (Hock 2005: 366). The incoming longwave radiation is emitted from the surrounding terrain and particles in the atmosphere, mostly water vapour, carbon dioxide and ozone. The part originating in the atmosphere is therefore highly dependent on the cloudiness and the amount and temperature of the water vapour (Hock 2005: 372). Furthermore, due to the strong absorption by water vapour, it is mainly determined by the conditions within the lowest few hundred meters in the atmosphere (King et al. 2008: 75). This makes clouds with their high emissivity an important source of energy to the snow surface. The surrounding terrain affects the longwave radiation on the one side by obstructing the sky and decreasing incoming radiation (like for the shortwave radiation) and on the other side by emitting additional radiation itself (Hock 2005: 374).

The effect of clouds on the surface energy balance is opposite for long- and shortwave radiation. King et al. (2008: 76) point out that on snow with its high albedo, the loss of shortwave radiation due to cloud cover is usually less than the increase in longwave radiation. In polar regions, where sun angles are low and cloud transmissities and albedo are high, this situation of increased energy input due to clouds is most likely to occur. The same is identified by Zhang et al. (1996: 2121) as they show that thin and low clouds have a more positive effect on the snow surface energy

balance than high and thick clouds. Because snow albedo decreases with time, they conclude that the effect of clouds on snowmelt is generally high in the early melting season while it decreases later on. The onset of snowmelt occurs significantly earlier under overcast than it does under clear sky conditions (Zhang et al. 1996: 2121).

3.2.5 Turbulent heat fluxes

The turbulent heat fluxes in the energy balance (formula 1) represent another source of energy to the snow surface. The fact that snowmelt depends on air temperature indicates the importance of turbulent heat transfers. Both, latent and sensible heat fluxes, increase with wind speed above the surface and the difference between the air and the surface regarding the respective value – temperature gradient for sensible heat and vapour pressure gradient for latent heat (Gray & Prowse 1993: 21). Hock (2005: 365) points out that strong temperature gradients can develop immediately above the snow surface because of its high thermal emissivity and the limitation of snow temperature to less than 0°C. These temperature gradients can lead to a stable air stratification and hence suppressed turbulent heat exchange (Hock 2005: 365).

Sensible heat flux to the snow surface is provided by the air immediately above the surface and by rain falling on the snowpack. The latter is particularly interesting because it may also produce latent heat fluxes. When rain falls on snow with a temperature below 0°C, it will first release sensible heat until it reaches the freezing point – the specific heat capacity of water of $4.218\,\mathrm{kJ\,kg^{-1}K^{-1}}$. Then the water freezes and releases the latent heat of fusion of $334\,\mathrm{kJ\,kg^{-1}K^{-1}}$ (Hock 2005: 366). If the snowpack is isothermal at freezing point, the water will only release its sensible heat (Dingman 2002: 199f; Gray & Prowse 1993: 22). In both cases, rain means a positive energy flux towards the snow surface and contributes either to the warming or the melting of the snowpack. When the rain does not freeze the latent heat of fusion is not released, making rain more effective for warming than for the melting of snow.

A related situation occurs when the low thermal conductivity on snow (chapter 3.1.2) allows melting in the upper snowpack during the warming phase, which is before the snowpack is isothermal at 0°C. The meltwater percolates deeper into the cold snowpack and refreezes (French 2007: 239). The released latent heat of fusion again contributes to the warming of the snowpack. Therefore, this process can be seen as vertical transportation of latent heat during the warming phase. As a consequence the refrozen water forms ice in the lower snowpack and may lead to formation of basal ice layers which are laid open in the late melting period and complicate the snowmelt-runoff relationship (French 2007: 239).

With respect to the latent heat fluxes, also evaporation and condensation need to be taken into account. The latent heat of evaporation is 2501 kJ $kg^{-1}K^{-1}$, which is much higher than the latent heat of fusion that is needed for the melting of snow (Hock 2005: 366). Therefore, condensation of water vapour onto the snow surface is an important source of energy for warming or melting of snow. The same applies to deposition of water vapour as surface hoar which naturally depends on a surface temperature below 0°C (Hock 2005: 366). Both processes are supported by the high thermal emissivity of snow which may result in low surface temperatures and therewith low water vapour pressure – especially under clear sky conditions. In turn, evaporation and sublimation reduce the energy available for melting.

The sublimation of snow should be highlighted in the context of its redistribution by wind as it is described in chapter 3.1.1. During blowing snow, high rates in sublimation occur due to the high ratio of particle surface area to mass, the excellent ventilation of the snow particles and and a generally higher atmospheric water vapour deficit because of atmospheric mixing by wind (Pomeroy et al. 1997: 1453). Sublimation is highly variable and difficult to quantify, but studies suggest a loss of 10–50% of the winter snow cover due to sublimation (Stone et al. 2002: 10-4f). When referring to spring snowmelt this means that the water equivalent that generates runoff is generally less than the total amount of winter precipitation.

In regions where the snow cover develops patchy patterns during the season, the local scale advection of sensible heat can significantly contribute to the point energy budget of the snow surface (Liston 1995). Snow-patches and snow-free areas show large differences in surface physics that arise in albedo and hence, surface temperature. Local advection of sensible heat from the snow-free areas with low albedo to the snow-patches can provide additional energy for melting as it is shown in figure 4 (Marsh 1999: 2124f). The effect increases with wind speed and depletion of the snow cover, but also with decreasing size of the single snow-patches (Liston 1995; Neumann & Marsh 1998).

According to e.g. Gray & Male (1981: 395), the geothermal energy as ground heat flux can be safely neglected for short-term periods when referring to the melting of the snow cover. Compared to other energy fluxes it makes up an insignificant part in the energy balance. The temperature at the bottom of the snowpack is indeed influenced by the ground heat flux, but the major contribution is given by storage of heat from summer warming (McClung & Schaerer 2006: 52). This warms the basal layer to or close to 0°C and can result in a strong temperature gradient within the snowpack and promotes temperature-gradient metamorphism when air temperature is low. The snowpack temperature data (chapter 5.3) will confirm that the basal snowpack temperature is significantly higher than in the upper snowpack and above the snow surface.

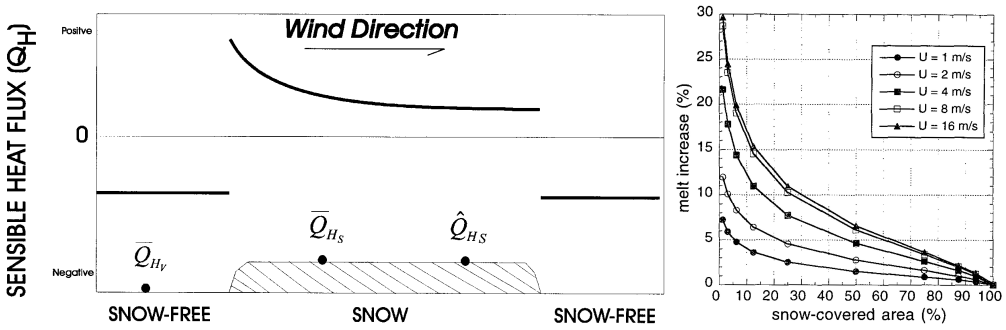

Figure 4: (a) Changes in sensible heat fluxes for snow-free and snow-patches by local advection. Negative flux is from surface to atmosphere and vice versa for positive flux (Neumann & Marsh 1998: 1548). (b) The related melt increase at different wind speeds (Liston 1995: 1711).

3.3 The role of snow in Arctic ecosystems

Snow is the dominating form of precipitation in the High Arctic and is of major importance to these ecosystems. Its relevance can be assessed on two different scales. First, the snow cover duration and spatial extend drives one of the most important positive feedback mechanisms in global climate change as pointed out e.g. in the IPCC Assessment Reports (e.g. Anisimov et al. 2007; Randall et al. 2007). Second, its character of thermal and optical insulation of the ground beneath and the storage and release of water affect not only geomorphology and hydrology, but also flora and fauna.

The global Climate Change has gained large attention in present research activities and with it the albedo feedback of snow covered landscapes and sea ice coverage in cold environments. This mechanism amplifies warming at high latitudes and makes these ecosystems exceptionally vulnerable to global warming (Meehl et al. 2007: 770–772). Its importance is manifested in many studies that use global circulation models to assess the future climate change. Randall et al. (2007: 638) point out that the poleward retreat of snow and sea ice is a robust feature of climate model projections. This leads to an increase in absorbed solar radiation and therewith, to higher temperatures in the lower troposphere. Modelled values for the reduction in annual mean snow cover of the northern hemisphere in the late 21st century are in the range of 9–17%, depending on chosen model and emission scenario (Meehl et al. 2007: 772). This comprises the poleward retreat of snow cover, decreased fractional snow coverage during winter as well as a shortening of the snow season with a later beginning and earlier ending (e.g. Stone et al. 2002; Meehl et al. 2007: 772). Despite the intensive research efforts, quality and strength of the feedback are not fully understood. Although temperature is a major driving force other feedback

mechanisms and atmospheric processes like cloud cover and circulation patterns, but also ocean heat transport, complicate relationships. Accordingly, model projections vary widely due to complexity (Randall et al. 2007: 638f).

The hydrological and physical characteristics of snow act a part in many geomorphological forming processes in periglacial environments. According to Blümel (1999: 172f), they can be grouped to fluvial processes, aeolian processes, as well as denudative and structuring processes which are all linked to the presence of snow or its melt water. When referring to Svalbard, fluvial processes are fully dependent on snow and glacier meltwater runoff and are therefore absent in winter (Blümel 1999). This main hydrological feature also controls aeolian processes since the adhesion of soil materials changes with the presence of moist. A complete analysis of geomorphological relevance of snow cover and melt goes beyond the scope of this thesis and will therefore be limited to the some unique periglacial processes.

Besides its fluvial (linear) erosion and forming, snow meltwater also acts directly beneath the snow cover leading to slopewash processes. These may be linked to the forming of hollows under perennial snow-patches (French 2007: 238f). Also to solifluction, the presence of water is essential: the rate of frost heave that leads to the typical see-saw downwards movement depends on the moisture content when the active layer freezes (French 2007: 54, 252f). Additionally, the expansion of freezing water drives the underlying structuring processes of sorted circles or ice wedges (French 2007). But the special relevance of snow in this context is rather due to its insulating character. The low thermal conductivity and temperature limitation to less than 0°C averts any melting of frozen ground underneath the snowpack. Thus, the timing of spring snowmelt is crucial to processes that base on seasonal or diurnal frost-thaw cycles. This comprises e.g. solifluction, the forming of patterned ground and ice wedge development, and generally the thawing of the active layer (Blümel 1999; Christiansen 2004: 164). A shorter duration of snow cover increases the summer active layer thickness and is connected to its erosion. In context of climate change, the response of permafrost to changes in not only air temperature but also snow cover is an important subject of research (e.g. Meehl et al. 2007).

Blümel (1999) outlines how local snow cover affects vegetation. He points out that the variety in snow cover duration on small scale results in a diverse vegetation cover in the Arctic tundra. A late melting in spring delays the onset of the growing season, but it protects plants from frost and dehydration. In their study on snow–vegetation relations in eastern Greenland Buus-Hinkler et al. (2006: 245) find that the timing of snow cover is of even higher importance for the time of peak vegetative activity than temperature. Figure 5 exemplary shows their result for snow cover depletion in relation to vegetative activity in northeast Greenland for spring 2003.

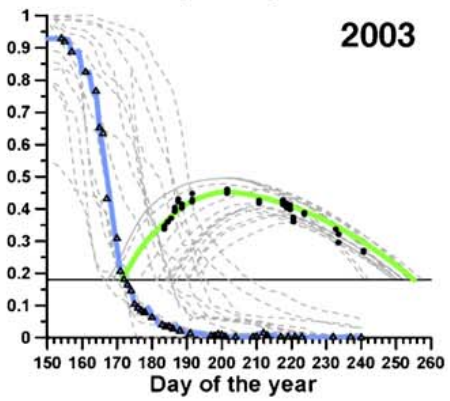

Figure 5: Snow cover depletion and vegetative activity in spring 2003 in Zackenberg, northeast Greenland from measurements by (multispectral) camera images. Black markers represent single measurements; blue line represents SCA; green line is vegetative activity (as NDVI); toned curves represent all years from 1988 to 2004 (Buus-Hinkler et al. 2006: 243).

But also winter snowpack thickness is of relevance to vegetation – only few species can survive on exposed spots that are prone to snow erosion by wind. When snow cover thickness decreases, this can directly limit growth by frost dehydration. Furthermore, a snow cover induced change in active layer thickness can affect the depth of the moist horizon right above the permafrost table (Blümel 1999: 165).

Animal life is affected by variations in snow cover characteristics e.g. through the accessibility of food. The Svalbard reindeer population, for instance, is vulnerable to the forming of ice layers within the snowpack that develop when rain falls on a cold snowpack (e.g. Bore et al. 2009: 6). In their study on dynamics in a specific Svalbard reindeer population, Solberg et al. (2001) find a large dependence of reindeer mortality on varying winter climate such as precipitation that leads to ice crust formation. Altogether the timing and characteristics of snow cover can certainly be named the most important factors to the biota in High Arctic ecosystems.

4 Materials and methods

4.1 Digital camera images

The camera used for the analysis is an automated digital camera that is placed on the eastern side of Linnévatnet near to its south end. The camera is a Pentax K110D that sits in a protecting case behind a glassed opening. It is solar powered and takes two images a day – 11:00 and 16:00 – which are saved in the JPEG file format onto a standard memory stick. The resolution of the

(a) **(b)**

Figure 6: (a) Time-lapse camera and (b) its image section exemplary shown as the 30 June picture.

images is 3008 times 2000 pixels. The camera is in automatic mode, so that it chooses the right exposure time and F-number for not over- or underexposing the pictures. Christiansen (2001) uses a similar setup and provides further information on components and construction.

The wooden case sits directly on the boulders on a basalt ridge (figure 6 (a)). The map (figure 1) shows place and viewing angle of the camera. Its view covers a triangular shaped area in Linnédalen. Linnévatnet (the lake), the sky and some boulders in the foreground take up a lot of space on the images (see figure 6 (b)). As a result, only one third of the image caption can be used for the analysis. Originally, the camera was installed to watch the changing of size, form, position and colour of the plume at the lake's inlet.

4.2 Processing of the digital camera images

The basic idea how to extract data about the snow covered area from the digital camera images (DCI) is to apply a "threshold filter" on the brightness values in each image. Every pixel showing lower greyscale values than this certain threshold is changed to black colour, pixels with higher values are changed to white. The outcome is a binary type image with one class referring to as snow and one class as non-snow or bare ground. Try-outs showed that this is a good option for separating snow from other surface types in the images. Similar studies use the same or a related approach (e.g. Schmidt 2005, 2007; Hinkler et al. 2002, 2003).

After this classification is applied, an image analysis tool is used to count the pixels in each class. The ratio of snow-pixels to total pixels can be interpreted as the snow covered area (SCA)

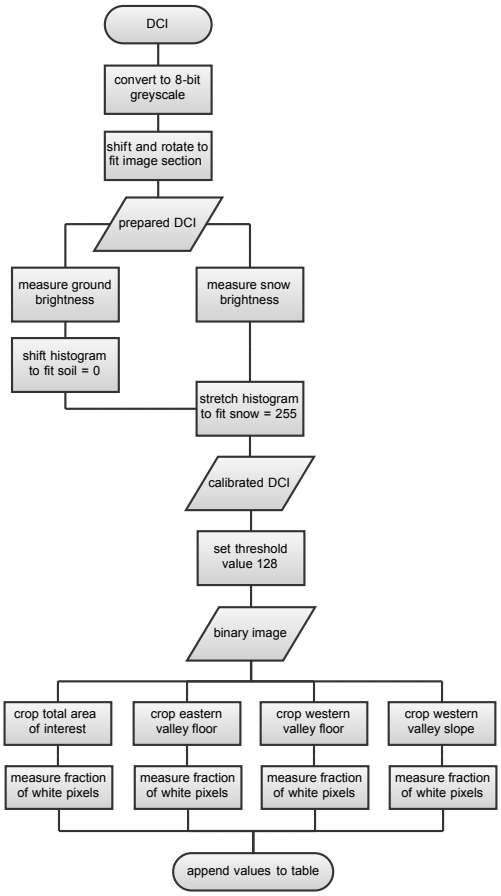

Figure 7: Flowchart diagram showing the image analysis procedure for a single DCI

as fractional value between 0 and 1. Doing this for a time-series of pictures throughout the spring allows to plot the SCA on a time scale. Data quality, the relation of SCA and snow water equivalent and the influence of perspective bias will be discussed in chapter 7.

The way of analysing the DCIs is shown in figure 7 as a flowchart-type diagram. The process can be summarised in a couple of steps that will be described in the following chapters:

1. Select a timeframe that covers the spring melt and exclude pictures with low clouds, fog or water drops on the glassed opening
2. Prepare the images to suite the analysis; particularly the adjustment of image orientation
3. Apply a convenient greyscale threshold to the images
4. Count black and white pixels in the area of interest in every image to gain SCA-data

4.2.1 Definition of the spring melt timeframe

In mid-latitudes the period of snow depletion is often interrupted by snowfall events and it can be difficult to make out a precise extend of the "spring". In high latitudes, the distinction between accumulation and melt period is usually sharp (e.g. Liston 1999). This benefits the definition of the timeframe for the image analysis. The starting point is 17 May 2008, which is shortly before there is any change in SCA visible in the pictures. The last image in the time-series is 11 August, when the cameras memory stick was downloaded because the fieldwork ended. However, this date fits good to the ending of the melting season. The camera takes two pictures a day, on 11:00 and 16:00. Only the 11:00-pictures are used for analysis for two reasons: 1) the time difference of only five hours would result in an uneven distribution of images in the time-series and, more important, 2) the 16:00 images show more shadows on the western valley slope than the forenoon-images.

Some of the images show water drops on the glassed opening of the camera case which result in a blurred picture. The affected days are excluded from the analysis. Same applies to days where low clouds or fog block the camera's view. The respective dates are listed in the results chapter. This is a problem of all methods that use terrestrial photography and the visible spectral band and is handled in the same way e.g. by Hinkler et al. (2002) and Schmidt et al. (2009).

4.2.2 Preparation of the images

The camera case sits directly on the ground on a basalt ridge. Because its original purpose was of qualitative type there was no good reason to prevent it from moving slightly. Hence, it is not fixed to stable ground. Thus, during the spring, water in the active layer melts. This results in surface lowering and moving of the stones the case is placed on. Since the camera moves a little, the image caption is shifted. This is not a big deal when the images are used for a qualitative analysis, but in this case some regions will be cropped to the nearest pixel (lake, sky and foreground) and the results should be as precise as possible. Hence, for all images, respect to this little motion is taken by using standard image editing software for moving and rotating the image to fit the position the camera had on 13 July 2008. To speed up this time-consuming correction of image orientation, an option could be a semi-automatic strategy using a matching-procedure similar to Schmidt (2007).

The raw RGB 24-bit JPEG type images are converted to 8-bit greyscale type represented by values from 0 to 255. This allows a straightforward classification of snow by the single-pixel brightness (e.g. Schmidt 2005). For a readily prepared image see e.g. figure 9. The use of

individual color channels or multispectral terrestrial photography as it is done e.g. by Hinkler et al. (2002, 2003) will be taken up in the discussion, chapter 7.

4.2.3 Image brightness standardisation and convertion to binary type

Standard image editing software offers a "threshold filter". This filter reclassifies the image using the brightness of every single pixel. Darker pixels are changed to black, brighter pixels to white. The brightness-value that that is used as threshold has to be adjusted between 0 (black) and 255 (white) for 8-bit images. For many of the pictures, 128 or rather 50% mid grey is a good value. It works fine under grey, cloudy weather conditions. Sunshine makes the whole image brighter and produces some shadows at the same time (figure 8). Further, snow has a high albedo which results in a higher overall brightness. In both cases the camera responds with a shorter exposure time for not overexposing the image. This again reduces the brightness of snow and bare ground in the images and hence, the threshold needs to be smaller (Schmidt 2007: 74). Accordingly, the proper threshold has to suite the unique conditions in every single image. Other studies using similar methods, e.g. Schmidt (2005, 2007), encounter the same problems.

The first approach was to manually find a proper threshold for every single DCI as it is also done by Schmidt (2007: 77). This not-so-satisfying way largely depends on the manual accuracy. Therefore, it is substituted by a calibrated method that takes the brightness of the individual images into account. This principle is also used by Corripio (2004) who extract surface albedo data from terrestrial DCIs. To gain information on individual image brightness, a snow-patch that outlives the complete melting period is chosen as well as a spot showing bare ground in the very beginning of the time series (figure 9). Both, the brightness of the snow-patch and the brightness of bare ground are assumed to be representative for the respective surface type at the time the specific picture was taken. The measured areal mean values of brightness of the spots are used to standardise the individual images to always similar brightness of the two surface types. This is performed by shifting and stretching of the image histogram using the calculation in formula 3, where I represents individual pixel brightness, G is bare ground brightness and S is snow brightness in each image. Values are limited to 0 – 255.

$$I_{new} = (I_{old} - G) \cdot \left(\frac{255}{S - G} \right) \tag{3}$$

The outcome is a set of images that all have the same brightness of snow and bare ground respectively. This allows to use a standardised threshold for the classification. In this case, the centre between them, meaning 128, gives good results. The quality of this threshold and the overall

(a) 6 June - prepared

(b) 29 July - prepared

(c) 6 June - transformed histogram

(d) 29 July - transformed histogram

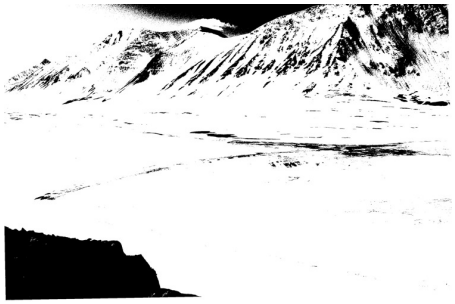

(e) 6 June - threshold applied

(f) 29 July - threshold applied

Figure 8: Analysis procedure on two images with different lighting conditions. 6 June (left) and 29 July (right) DCIs after preparation (a, b), with transformed histogram (c, d) and applied threshold (e, f).

classification performance will be discussed in chapter 7. Figure 8 shows that this method can handle very different lighting conditions.

4.2.4 Identification of the area of interest

Some regions in the DCIs are not interesting for studying the snowmelt process. Naturally, the sky is one of them, but also the parts that are covered with water are not taken into account.

The snow on the frozen lake melts under very different conditions and does not play a role for water runoff here. The boulders on the basalt ridge in the foreground are too close to the camera to give useful results. Furthermore, the cirque on the picture's right end is heavily affected by shadows. The higher part of the valley's western slope is frequently covered by clouds. Hence, these areas are cut out to prevent problems with the analysis. Because the lake's heat capacity may affect the melting process in some way, the small stripe of land between the lake and the bottom image border is excluded as well. Due to the perspective bias it makes up a large area on the pictures although it is only a couple of meters wide. On the western valley slope, some small ridges frequently cast shadows and the affected areas are also excluded. The leftover makes up approximately one third of the original image area and can be described as "the valley floor and lower parts of the western slope". Figure 9 shows the area used to calculate SCA values. In the alpine valley Lötschental, Switzerland, Schmidt (2005, 2007) also encounters the problem of shadows on the valley slopes. She masked the affected areas and used a separately adjusted threshold value.

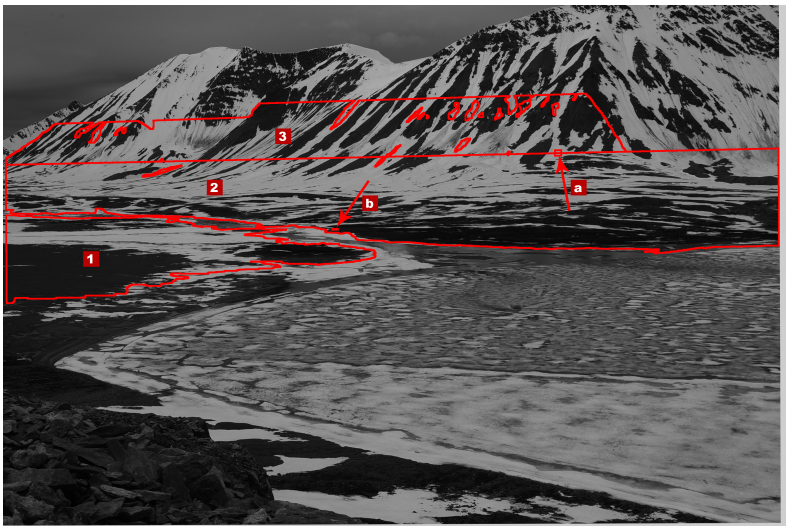

Figure 9: Prepared image showing the area of interest and the spots used to measure snow and ground brightness for calibration. (1) represents eastern and (2) western valley floor; (3) is the western valley slope; (a) represents the spot used to measure snow brightness and (b) ground brightness.

4.2.5 Calculation of the snow covered area (SCA) fraction

To allow a detailed analysis of the snowmelt it is beneficial to have a spatial differentiation within the area of interest. It is interesting to study regions separately because the snow distribution depends on the topography and wind drift plays an important role. Additionally, these regions are differently exposed to the camera. The western slope is tilted and is therefore better exposed

than the valley floor on the western side. The eastern valley floor is closer to the camera than the western one. This has to be taken into account as otherwise the foreground is weighted higher in the results. It will be discussed in chapter 7 whether this is a proper way of respecting the perspective bias. Figure 9 shows the separation that is chosen for analysis.

Other studies on the depletion of snow cover, e.g. Hinkler et al. (2002), use similar separations of their area of interest. Hinkler et al. (2002) divide their area in three sections based on elevation above sea level while Schmidt (2005, 2007), Schmidt et al. (2009) use a digital elevation model to make out not only elevation bands but also areas of different exposition, shading, inclination, etc. Both could not be accomplished here due to a lack of high resolution elevation data.

Since the images at this point contain information about the surface type of each pixel, the ratio of snow- to total number of pixels is referred to as SCA. The calculation is performed for the three areas separately and for all images in the time series. Together with the image timestamps, the SCA data for the total area of interest and the three separate regions can then be plotted over time.

All measurements, calculations and transformations on the images, except the corrections to the image section, are performed using ImageJ. This is a public domain image processing program that is freely available from http://rsbweb.nih.gov/ij/ (Collins 2007). It is developed at the US National Institutes of Health and is actually used for biological purpose like microscopy. ImageJ has the ability of scripting and batch-processing images and can perform the calculations and measurements with tabular output. For further information on the program and its use see Collins (2007).

4.3 Measurements on the snow-patch

The image analysis calls for being combined with reference data in some way as otherwise the SCA data does not give any information about the decrease in snow water equivalent – which is of high interest when referring to meltwater runoff and related processes. The fieldwork in Linnédalen allowed to arrange a set of measurements on the snowpack, but at this point the main part of the melting event was already over.

The measurements are taken on a snow-patch on the lower western valley slope, which is well exposed to the digital camera. The snow-patch is shown in figure 10 and its position is marked in the map (figure 1). The measurements that are set up as a time series are taken every other day between 26 May and 9 August 2008. They are described in the following chapters.

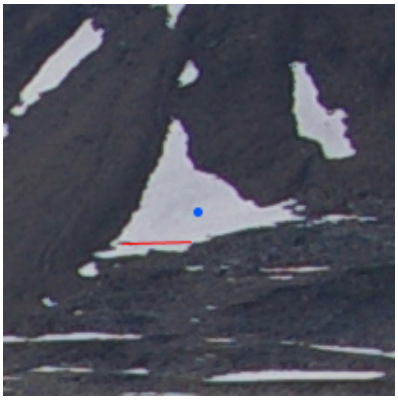

Figure 10: The snow-patch that was chosen for the measurements seen by the digital camera on 24 July. Blue dot represents the snow depth stakes; red line is the transect for depth measurements. Note that the shape is transformed by perspective bias.

4.3.1 Exposure

The exposure of the snow-patch is documented based on two different aspects. The direction of exposure and inclination is taken using a compass and an inclinometer. Furthermore, the solar shading of the snow-patch caused by topography is documented. As described earlier, radiation is one of the major energy sources for melting of snow and varies a lot with exposure. The solar shading by the surrounding terrain reduces the incoming shortwave radiation from sunlight and as diffuse radiation from the sky. Additionally, the terrain plays a role for the longwave radiation coming from the atmosphere but also from the surrounding landscape (Hock 2005: 366, 368).

4.3.2 Snow-patch size

The snow-patch's shape can be described as "approximately right-angled triangular" (figure 10). It keeps its shape while melting during the period of measurements that are taken every other day. It is not known whether it outlived the summer or even several years. For getting an approximate size value, the side lengths of the triangle are measured. The maximum extends of the snow-patch in the respective directions are taken as corners of a right-angled triangle to approximate the areal extend.

4.3.3 Snow depth, density and water equivalent

On the snow-patch in Linnédalen the snow depth is measured every other day using two different setups. The depth is taken and averaged in five points in center of the triangular shaped patch.

The points are spread within approximately 0.5 m^2 and the stake is removed after gauging to avoid radiation from it. As a convention, the snow depth is not measured orthogonally to the snow surface but vertically (American Avalanche Association 2010: 14).

Additionally, snow depth is measured along a transect in the lower part of the patch. Values are taken every meter on both sides, an arm-length away from always the same track. Figure 10 shows the locations of the measurements on the patch.

The snow water equivalent (SWE) is the actual amount of water stored in the snowpack. It is expressed as vertical depth of the water layer if the snow would be melted. Hence, it is measured in millimetres like liquid precipitation (Brown & Armstrong 2008: 187). A vertical density measurement (ρ) and the snow depth (d) are necessary to calculate the SWE:

$$\mathrm{SWE} = \rho \cdot d \tag{4}$$

The density is taken using the gravimetric method for the whole snowpack at once. This eliminates information about the layering of the snowpack but it provides a correct mean value. A vertical column of the snowpack with a known volume is weighted; the standard unit is kg m^{-3} (e.g. Brown & Armstrong 2008: 187).

4.4 Monitoring of the snowpack temperature

The sensors are deployed on the eastern side of Linnéelva, just beside the river, approximately on half way between Linnévatnet and Linnébreen. It is a 45 cm stake that is vertically fixed in the ground. On 7, 15, 30 and 45 cm above the ground it has horizontal branches that are equipped with Hoboware sensors on them. These measure brightness (horizontally directed) and temperature every 30 minutes. With increasing snow depth, the sensors successively get buried and they provide information about temperatures within the snowpack. The resolution of snow depth values obtained by the four brightness sensors is too coarse to be useful for analysis. Therefore, the data is only evaluated regarding snow temperature in the different depths.

4.5 Weather station data

A Hoboware weather station on the valley floor provides numerous weather data for the valley. It is situated near the south end of the lake (figure 1). The following weather elements are measured on a 30 min resolution:

- air temperature (°C)
- soil temperature (°C) in 0.5 m and 1 m depth
- liquid precipitation (mm)
- wind speed ($m\,s^{-1}$) and direction
- air pressure (Hg)
- solar radiation ($W\,m^{-2}$), up- and down-looking

The humidity sensor was out of order during the period of measurements due to a malfunction. The liquid precipitation values have to be carefully considered because snowfall measurements in such gauges are highly affected by wind (e.g. Dingman 2002: 169f) and meltwater in the gauge produces positive precipitation data.

Additionally, a temperature logger is placed on the western valley slope, on top of the moraine of the cirque on the slope of Griegfjellet, just southwest from the lake's southern end. It is hidden underneath a radiation shield and measures temperature and air humidity on a 30 min scale. It is taken into account in addition to the main weather station because it is situated closer to the snow-patch with a comparable exposure.

5 Results

5.1 Snow cover data and digital camera images

The DCIs are analysed from 17 May to 11 August 2008 – fitting the first visible changes in SCA in the beginning and the end of the main melting season. The slight moving of the ground that affected the image caption by moving the camera case happened between 15 June and 13 July 2008. The foreground in the bottom left of the images shows the stones creeping. This happens before the camera case actually moves, between 26 May and 10 June.

Bad weather conditions with low clouds blocking the cameras view or parts of it take effect on the analysis. Since clouds have a high reflectance they are classified as snow-type surface by the presented method. Water drops on the glassed opening of the case blur parts of the image and also affect the results. For both reasons 19 of the 87 images are not taken into account, leaving 68 images for further analysis. This is still significantly better than in other studies with an area of interest that has a larger vertical extend – e.g. Schmidt (2007), Schmidt et al. (2009). The respective dates are listed below.

- May: 29–31 (low clouds)
- June: 1 (very low clouds and fog), 2 (water drops on the glass), 22 (clouds and water drops)
- July: 1 (water drops), 4 (very low clouds), 5 (low clouds), 9 (low clouds), 11 (water drops), 12 (water drops and clouds), 19 (water drops), 21 (water drops), 27 (low clouds)
- August: 1–4 (low clouds and fog)

5.1.1 Image brightness of snow and bare ground

As described above, the brightness of snow and bare ground is measured in every image to allow a adequate histogram transformation to standardise image brightness. Figure 11 illustrates the mean brightness in the measured spots. It demonstrates that images have different brightness characteristics changing not only with time but also due to individual daily conditions. As it is discussed in chapter 7, the increase with time is due to changing of the SCA fraction that influences overall reflectance and therewith image brightness. The brightness threshold for classification of snow and ground naturally lies between both values. Here, actually the centre between both is used as it is shown in black in figure 11. However, it is applied after the individual brightness standardisation so that it is always 128 (as the middle of the given greyscale range).

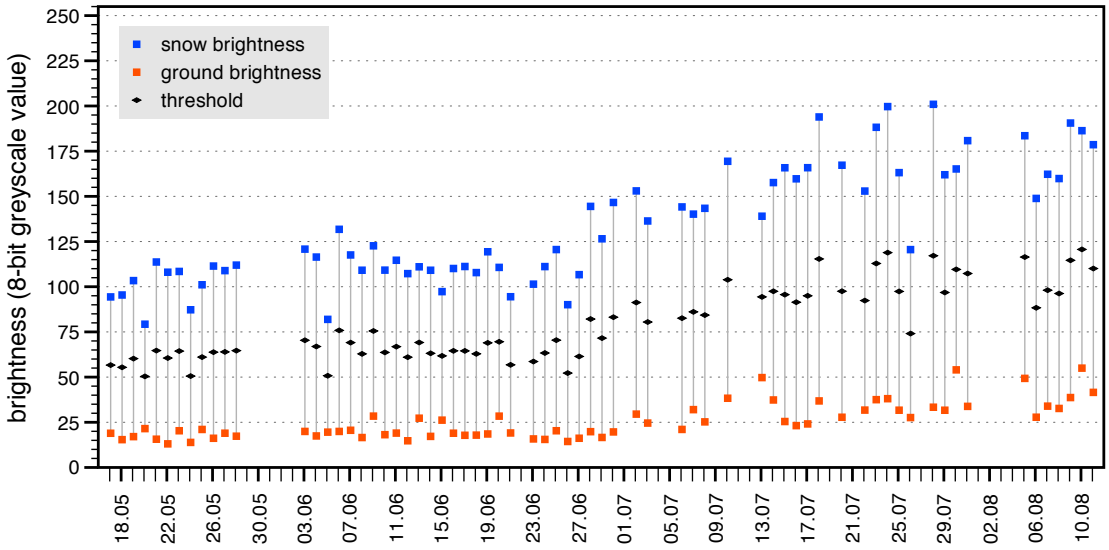

Figure 11: Differences in the brightness of snow and bare ground in the image analysis. Black markers represent the threshold used for classification. Note that 8-bit values range from 0 (black) to 255 (white).

An interesting approach is given by Corripio (2004) who uses similar data to obtain spatial information on surface albedo. He uses reference points with know (measured) albedo in the field and compares them with the brightness registered by the camera (like figure 11). By applying various correction procedures he then gains reliable data on surface reflectance.

5.1.2 SCA fraction data

Figure 12 illustrates the results obtained through the image analysis. The SCA fractions for the three areas are given separately to show spatial differences in snow distribution and the melting process. A spatial mean value for the total area of interest is given as the black dashed line. The images that are excluded due to weather conditions are not represented by any value. Numerical values are given in the main results table (A-1).

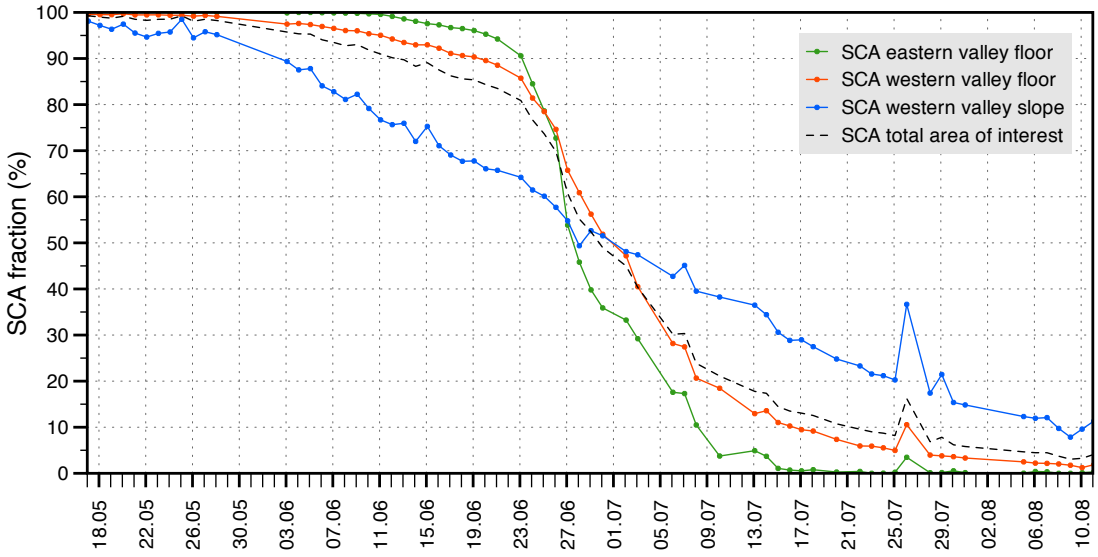

Figure 12: SCA data for spring 2008 obtained through image analysis.

The dataset shows how the snow cover melts throughout the spring. In the beginning, snow coverage is nearly complete. It then depletes with increasing and later with decreasing speed. In relation to similar studies the plot shows a snow depletion curve that is typically S-shaped but with a relatively high temporal resolution (e.g. Christiansen 2004: 161; Hinkler et al. 2002: 4679). The differences between the three areas and especially the role of the almost linear decrease of SCA on the western slope will be studied in the analysis, chapter 6.

5.2 Weather station data

Due to the high temporal resolution of the sensors, the weather station dataset is quite large and unwieldy. To allow an analysis in combination with the SCA data, values are aggregated to daily sums or averages. The following data is taken into account:

- precipitation as daily sum
- temperature as daily average
- wind speed as daily average
- albedo as calculated daily average of the ratio of down- to up-looking radiation values

The results are given in the main result table (A-1). Precipitation values generally are low which is in line with the climatological data from Isfjord Radio. Here, the monthly precipitation minimum is in May (see climograph, figure 2). Within the time series, the daily maximum of 22.4 mm occurred on 7 July and some other short wet-spells around 2 June, 22 June and 10 August as well as some single-day events.

The daily average of temperature is calculated by taking the real average from all values per day. No values are weighted higher than others in the calculation as it is done for other purposes. Hence, the data represents the actual sensible heat provided by the air two meters above the ground, which is then available for turbulent heat fluxes. Temperature is highly variable but increases through the time series. The coldest day during the analysed period is -3.15°C on 19 May and warmest is 23 July with 10.15°C.

Albedo decreases from more than 0.8 in the beginning of the time series to less than 0.2 on 22 June, which is likely to represent bare ground rather than snow (figure 13). This is in line with the findings by Gerland et al. (1999: 2339) that are given in figure 3. It should be noted here that the calculated ratio of down- to up-looking radiation values does not give the same quality results as the equipment used by Gerland et al. (1999), but should be sufficient in this context.

5.3 Snowpack temperatures

The snowpack data consists of temperature and radiation values on a 30 min resolution. For usability reasons, they are scaled down to daily averages. The radiation sensors are directed horizontally, so that the values can not be taken as proxy for albedo. Further, the sensors have a fairly coarse vertical graduation (7, 15 and 30 cm above ground). Thus, information about when snow depth decreases down to one of the certain depths is not very meaningful.

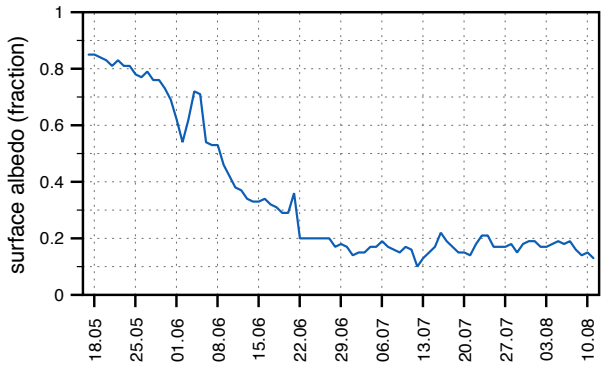

Figure 13: Measured surface albedo at the main weather station calculated as daily average of the ratio of down- to up-looking radiation values.

Table 1: Snowpack temperature 30 cm, 15 cm and 7 cm above ground from 1 May to 3 June 2008. Note that the stepwise temperature increase in the dataset originates in the graduated sensibility of the sensors.

	7 cm	15 cm	30 cm
	above ground		
01.05.08	-0.55	-1.00	-1.34
02.05.08	-0.55	-1.00	-1.34
03.05.08	-0.55	-1.00	-1.34
04.05.08	-0.56	-1.00	-1.34
05.05.08	-0.56	-0.99	-1.34
06.05.08	-0.56	-0.98	-1.34
07.05.08	-0.56	-0.97	-1.34
08.05.08	-0.56	-0.95	-1.34
09.05.08	-0.55	-0.90	-1.30
10.05.08	-0.55	-0.89	-1.23
11.05.08	-0.55	-0.89	-1.23
12.05.08	-0.55	-0.89	-1.23
13.05.08	-0.55	-0.89	-1.23
14.05.08	-0.55	-0.89	-1.23
15.05.08	-0.55	-0.89	-1.22
16.05.08	-0.55	-0.89	-1.15
17.05.08	-0.55	-0.89	-1.11
18.05.08	-0.55	-0.88	-1.11
19.05.08	-0.55	-0.84	-1.11
20.05.08	-0.55	-0.78	-1.09
21.05.08	-0.55	-0.77	-1.00
22.05.08	-0.55	-0.77	-1.00
23.05.08	-0.55	-0.77	-1.00
24.05.08	-0.55	-0.77	-0.96
25.05.08	-0.55	-0.77	-0.89
26.05.08	-0.51	-0.70	-0.89
27.05.08	-0.23	-0.59	-0.81
28.05.08	-0.21	-0.49	-0.71
29.05.08	-0.21	-0.44	-0.65
30.05.08	-0.21	-0.43	-0.56
31.05.08	-0.10	-0.28	-0.34
01.06.08	-0.10	-0.12	-0.10
02.06.08	-0.10	-0.10	-0.10
03.06.08	-0.10	-0.10	-0.10

The sensor on 45 cm above ground was broken off his branch at an unknown point during the winter, possibly by reindeer. This results in an unknown actual depth in the snowpack and other uncertainties. Its values are therefore not listed in the results and are not taken into account in the analysis. The other data is given in table 1. It shows how temperatures within the snowpack increase until it is isothermal at the melting point. The two upper sensors reveal warming from the beginning of June or earlier while the bottom one does not react until 26 May. The data will be used to make out the warming phase that marks the beginning of the hydrological melting period.

5.4 Measurements on the western slope

5.4.1 Exposure and solar shading

The exposure data for the snow-patch on the western valley slope, including aspect, inclination and solar shading, is taken in its centre on 28 July 2008 using a compass and an inclinometer. The aspect is east-northeast with an inclination of 28°. This results in predominant morning sun as incoming solar radiation.

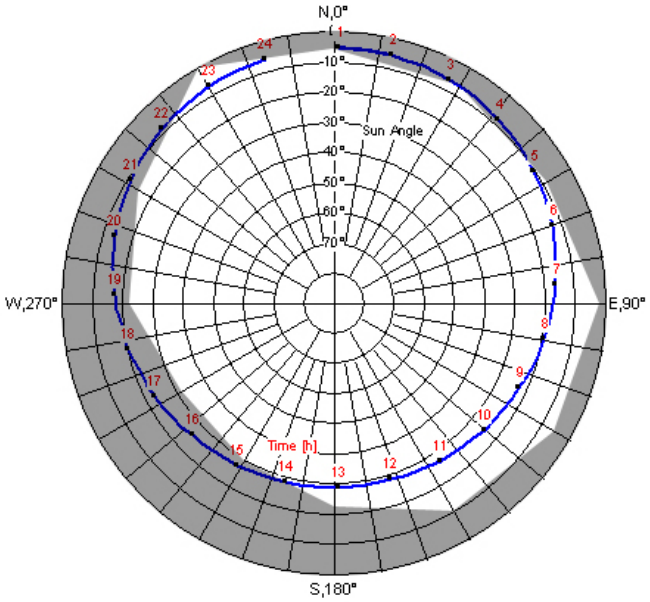

Figure 14: Solar shading of the snow-patch by surrounding topography. Grey represents terrain and the blue line represents the calculated progression of the sun on 2 August 2008. Numbers are hours of the day. Coordinates used for sun progression are 78° 01' N, 13° 48' E. Modified according to Flassak (2007).

The elevation is measured with a calibrated altimeter to avoid major barometric effects due to weather changes. On an elevation of 117.75 m a.s.l. the shading by the surrounding terrain still plays a major role. For instance Griegfjellet, on the back side of the snow-patch, blocks solar radiation throughout the afternoon and evening. Figure 14 illustrates the reduction of solar radiation by topography measured with the inclinometer in combination with the calculated progression of the sun.

5.4.2 Snow-patch size

The snow-patch's extend is measured every other day in horizontal and in upslope direction. The area is then calculated as $A = \frac{ab}{2}$ with the assumption that the shape is right angled triangular. Working on the small scale and the rocky and inclined ground make it difficult to determine the maximal extend of the snow-patch precisely. Additionally, the snow-patch successively changed its shape which causes further uncertainties regarding the size measurements. Table 2 shows how the snow-patch decreases in size. The data quality will later be discussed and contrasted with the snow depth measurements.

5.4.3 Snow depth, density and water equivalent

The first snow depth gauging setup consists of five measurements every other day that are averaged. This provides a clear dataset about the snow depth in the snow-patch's centre. The data is given in table 2 and shows that melting at this point is all but uniform. Thickness starts at 212 cm, and within 14 days it decreases to 138 cm.

The second method to obtain snow depth data is thought to provide a dataset with snow depth values along a given transect consisting of two times 16 points for each timestamp. The attached table (A-2) shows the mean value for every distance-metre from the starting point. Due to melting, the length of the transect decreases from 17 m to 3 m during the period of measurements. This limits data significance and is disadvantageous for the analysis. Since the first snow depth setup provides more reliable results, the data from along the transect is not considered in the analysis.

Density is sampled on 28 July 2008. A cylinder with given volume is pushed vertically through the whole snowpack near the centre of the snow-patch. The snow is weighted and the result is compared with the volume in a scaled cylinder after melting (room temperature). The coincident density is 393 kg m^3. According to Gray & Prowse (1993: 7.5) this is a rather high density for snow. It can be attributed not only to the settlement of snow cover and to winddrift but also to the

Table 2: Measured size and depth of the snow-patch, temperature and humidity from the nearby data logger on the western slope and (cumulative) precipitation and average wind speed from the main weather station. Note that the data logger values are averaged over the 24 h before the measurements are taken around 12:00.

	measured		data logger		main weather station	
	size (m^2)	snow depth (cm)	temp. (°C)	rel. humidity (%)	precipitation (mm)	wind ($m\,s^{-1}$)
26.07.08	2298.80	212.40			0	5.46
27.07.08			6.40	82.24	0	3.14
28.07.08	2065.55	195.00	4.03	93.30	0	2.69
29.07.08			6.23	89.19	0.4	5.16
30.07.08	1411.83	180.80	2.74	85.97	0	3.34
31.07.08			4.40	76.71	0	2.29
01.08.08	1419.60	173.20	7.49	69.33	0	3.63
02.08.08			3.22	95.77	0	1.71
03.08.08	1398.02	165.80	3.33	96.96	0	1.70
04.08.08			2.83	98.35	0	2.35
05.08.08	1312.16	154.00	6.26	81.80	0	4.68
06.08.08			3.88	78.93	0	6.80
07.08.08	1276.76	144.80	3.20	81.94	0	4.88
08.08.08			3.77	71.13	0.6	3.23
09.08.08	1242.78	137.60	3.96	86.57	2.4	2.25

storage of meltwater in its pore spaces (chapter 3.1.2). The density information can be used to calculate the SWE at the point where the density is measured. With a local thickness of 1.235 m the snowpack equals a local SWE of 486 mm.

5.4.4 Temperature and humidity logger

For a better comparability with the other measurements on the snow-patch, the temperature and humidity data from the western slope is averaged for the 24 hours before the measurements are taken in the field (approximately 12:00). This accounts for temperature changes e.g. in the afternoon which would otherwise be counted as if they occurred before the measurements are taken in noon. To complete the data on relevant weather elements, information on precipitation and wind from the main weather station is included in table 2. Although the latter is not handled in the same way, this should not cause major inconsistencies since the datasets are not directly compared.

The data reveals temperatures varying between 2.74 and 7.49°C which mirrors the late season. In contrast to the snow-patch depth and size measurements, temperature and humidity are given on higher resolution. The latter covers a period of rather high values from 2 to 4 August, which is in line with calm (windspeed from weather station) weather with low clouds (camera images) in the valley that also impede image analysis these days. Precipitation is very low with a sum of only 3.4 mm within the 14 days.

6 Analysis

6.1 Hydrological phases of the melting period

The dataset of SCA from 17 May to 11 August 2008 shows how the snow cover disappears from the valley floor first with increasing, later with decreasing speed. This leads to an S-shaped graph when the SCA is plotted over time. Ablation does fairly little progress in the period before and after the main melting event. During the main melting event, the major part of the snow cover melts within only a couple of days. The SCA depletion on the western valley slope is discussed separately, because it does not have that convex-concave shaped graph.

The time series starts on 17 May with a SCA of more than 99% on the valley floor. At this point, and also for the next couple of days, the weather station has not gauged any significant air temperature above 0°C since mid February. Positive temperature data and eventual melting earlier in 2008 has unlikely been of major extend and is not taken into account.

6.1.1 The warming phase

The temperature data from within the snowpack allows to tell precisely at which point the snowpack is isothermal. Due to the very low thermal conductivity of snow, it takes a while for the warmth to penetrate from the upper surface of the snowpack to the sensors in the bottom. Hence, the starting point of increasing temperature at the uppermost temperature-logger of the gauging setup does not indicate the exact beginning of the warming phase. The thermal conductivity increases non-linearly with snow density – e.g. $0.4\,\mathrm{W\,m^{-1}K^{-1}}$ for a $400\,\mathrm{kg\,m^{-3}}$ density snowpack (Langham 1981: 295ff). If snow depth and density values for this certain spot and time would exist, the time it took the energy to penetrate through the snowpack could be estimated.

The dataset of temperature in the snowpack (table 1) shows that the warmth comes from the upper snow surface. It reaches the uppermost sensor first, then the lower ones successively. The approximate dates of the beginning of warming in the respective depths are

- 7 cm above ground: 26 May
- 15 cm above ground: 10 May
- 30 cm above ground: approximately 26 April

These dates are hard to determine because the temperature increases fairly slow. The two upper sensors do not show real progress before 20 May. On 31 May, the snowpack's isothermal state is reached almost isochronous at the three sensors. Only the 15 cm sensor takes to 1June. This marks the end of the warming phase.

The warming of the snowpack requires energy, namely the specific heat capacity of snow of $2.009\,\mathrm{kJ\,kg^{-1}K^{-1}}$ (Hock 2005: 366). The precipitation gauge does not show any significant values for the respective period and hence, rain cannot contribute major amounts of energy in this period. The averaged air temperature does not rise above 0°C before 25 May. This results in weak sensible heat fluxes during this period, although higher wind speeds occurred from 21 to 23 May. Since albedo does not fall below 0.8 until 24 May shortwave radiation cannot contribute a lot of energy as well. This indicates that longwave radiation is the major source of energy available for the warming period before the 25 May. The DCIs support this hypothesis as they show overcast conditions from 20 May on, longing for the rest of the warming phase.

From 25 May on, daily air temperatures exceed 0°C and albedo drops down to 0.69 on 31 May. The pictures show fairly overcast conditions and low clouds for the rest of the warming phase indicating that longwave can exceed shortwave radiation energy input. A higher windspeed on the last two days of the warming phase and air temperatures of 1.58°C and 2.20°C on these days contribute some sensible heat flux. The local advection of sensible heat originating from snow-free patches is insignificant for the whole warming phase since SCA is still almost outright.

The clouds seem to contribute significantly to the warming. The beginning of serious temperature increase within the snowpack corresponds to the appearance of clouds. Very low clouds or fog in the valley dominate the weather conditions in the last two days of this phase, while temperatures rapidly rise within the snowpack – especially at the uppermost sensor. This significant role of clouds is in line with the outcome of Zhang et al. (1996) who studied the effect of cloud cover on snowmelt.

The last days of the warming phase show a flood event in the valley, starting on 28 May, lasting about ten days. It is not identifiable from the pictures where the water comes from. It shows up as a streamflow on the eastern valley floor running towards Linnéelva. On the 31st it increases rapidly in size and then covers the entire lake ice with water. Later, on 3 June it drains into the lake through a hole in the ice. Since the snowpack is not yet isothermal on 28 May, the pore

spaces can not be filled up with free water. This indicates that the water can not be meltwater from snow. The large amount of water speaks for a draining event, possibly of Krongressvatnet, which is situated up the eastern valley slope on an elevation of 99 m a.s.l. Several options for the water's origin were discussed in the field. Since the valley is still completely snow covered, the water drains through the snowpack. This fills up the snow's pore spaces reducing the amount of running water on the one hand side, but could also cause a feedback effect on the other side. Assuming that the water's temperature is above the freezing point it could provide sensible heat for warming the snowpack and then liberate latent heat when freezing, like it does when rain falls on cold snow. As soon as the snowpack is isothermal, the water's sensible heat would support melting. However, it is unlikely that the water's temperature is significantly above 0°C and furthermore, the non-isothermal state of the snowpack does not support the thesis of a snow-meltwater flood.

6.1.2 The ripening phase

As soon as the snowpack is isothermal, all energy input is consumed by melting snow. In spring 2008, this starts on 1 June, but it is difficult to determine at which point the snowpack is ripe since the setup of measurements does not contain instruments for measuring liquid water in snow. Additionally, the water from the flood event covers the channel of Linnéelva, making it hard to tell from the pictures whether runoff from snowmelt occurs or not. However, the optical properties of the snowpack change with its physical properties. The albedo of snow decreases with increasing liquid water content in the snowpack because it increases the effective grain size (Winther et al. 1999: 2036). Meltwater from the snow surface percolates down and fills up pore spaces in the snowpack. On 6 June the snow albedo drops from 0.71 to 0.54 and then stays fairly constant for three days. Afterwards it continues decreasing. Another drop in albedo occurs some days earlier, around 2 June, which is rather connected to (the measured) precipitation event since albedo increases back to 0.72 afterwards (figure 13). The precipitation gauge does not show values for 6 June that could cause a significant change in albedo. This may indicate that this drop in albedo marks the time where the maximum liquid water storage capacity is reached. The weather conditions change slightly from sunny to overcast but this should only have slight increasing effects to the albedo (Gerland et al. 1999: 2341) and did not cause significant changes when weather conditions changed earlier. Using the change in albedo as indicator to determine its ending, the ripening phase takes place from 1 to 6 June.

On the first two days of saturating the snowpack, there is no SCA data available because bad weather renders the picture analysis impossible. These two days show low clouds, humidity and

precipitation with temperatures > 2°C. The precipitation mainly falls on 2 June, rapidly affecting the albedo. From 1st to 2nd it drops from 0.62 to 0.54 due to the increased liquid water content. At this point, the snowpack is already warmed up. Therefore the rain does not freeze and liberate latent heat. Because the SCA data is missing for these days the contribution to snowmelt is insecure but probable.

The weather conditions are sunny on 3 June with an SCA of still 99.9% on the eastern valley floor and 97.5% on the western floor. Within the next two days, the value on the western floor decreases to 93.8% whereas it stays fairly constant on the eastern side. However, from the beginning of the ripening phase on, the SCA starts decreasing. As described above, albedo recovers after the rain event rising from 0.54 on the 2nd back to 0.72 on the 4th of June. This is likely because the amount of liquid water underneath the snow surface decreases as water percolates down when the amount of present water originating from the rain event exceeds the holding capacity of the snowpack.

6.1.3 The runoff phase

Until 21 June the decrease in SCA is small, represented by an average loss of approximately 0.5% per day only. From the DCIs, this period shows fairly variable weather conditions ranging from clear sky to overcast, but no precipitation except an insignificant, hardly measurable value on 11 June. Temperatures are relatively low during this time, ranging from 0.17°C to 2.07°C, causing only weak sensible heat fluxes. The major change for this period of 15 days arises in the albedo. From the 6th to the 20th of June it decreases from 0.54 to 0.29. At this point the albedo values must be handled with care since the bare ground also reflects shortwave radiation. Still, this is in line with typical albedo of melting snow cover (Gerland et al. 1999). Later in the season, when the snow is certainly gone, albedo varies around 0.15 to 0.20. As described above, the snowpack gets transparent to shortwave radiation when melting down to a certain depth. This decreases albedo significantly. Assuming that this is the case here this means that the weather station is now placed on an almost snow-free patch and the albedo values are now defective regarding their validity for the whole area of interest. Since albedo is 0.54 in the beginning of the runoff phase, which is already a fairly low value, it can be taken as “fairly low” from now on. On the 21st it performs a little jump to 0.36, which is very likely caused by changes on the bare ground surface. There is no obvious connection to other available data. Afterwards albedo reaches lowermost values. The meaning of this period until 21 June with only slow decrease in SCA will be discussed later since SCA is not a linear function of water equivalent.

Then, synchronous with the summer solstice, the main, rapid melt event begins. The weather station registered a rain event with 13.2 mm on 22 June, involving three more days with little precipitation. This is accompanied by a temperature jump to 3.38°C. These weather conditions promote melting as it is shown in the SCA data. Within the next two weeks SCA drops to 17.6% on the eastern and 28.2% on the western valley floor. This means a depletion of more than 60% SCA within only 14 days. Since the beginning of the runoff phase the albedo is low. This makes the snowpack more sensible to shortwave radiation. The rain event from 22 to 25 June and some other smaller events on 30 June and 3 July contribute to this fact. Air temperatures stay fairly high during this period, not falling below 2.8°C and reaching a maximum of 6.1°C. In addition, the effect of local advection of sensible heat starts to take place. Since the valley now shows a really patchy pattern of snow distribution, the low albedo of snow-free patches promotes local warming of air which then brings sensible heat to nearby snow-patches (Marsh 1999: 2124f). Furthermore, Gray & Prowse (1993: 22f) state that the melt of large snow-patches is mainly controlled by radiation and as they decrease in size, turbulent energy fluxes become the dominating source of energy for melting. From about 3 July on, this is likely to be the case here.

The period of rapid melt ends on 8 July with an SCA of 10.5% on the eastern and 20.7% on the western valley floor. A rain and wind event from 10 to 13 July reduces the snow cover on the western floor to 13.0% but does not have significant effects on the eastern side, since this is almost snow-free at this point. However, this rain event involves some slight snowfall on the slope of Griegfjellet, but with the snowline high enough to be out of range for the slope-area in the image analysis. On the valley floor the daily averaged temperatures remained above 2.3°C.

The precipitation event is followed by a number of warm days with temperatures up to 10.2°C (23 July). The SCA on the western side decreases slowly, reaching values below 5% on 28 July. The post-melt period, when SCA decreases slowly, will be analysed in detail in a separate chapter as it is covered by the measurements performed during fieldwork. Finally, it has to mentioned that one day stands out significantly in the dataset. On 26 July all SCA values show an increase that is connected to difficult lightning conditions challenging the method of DCI analysis (see chapter 7.1.1).

6.2 Spatial differences in snow cover depletion

6.2.1 Differences between western and eastern valley floor

The temporal decline in SCA shows the same S-shaped curve for both areas on the valley floor. Also changing weather conditions arise similarly in the SCA datasets of the western and the eastern valley floor. Nonetheless, they show different characteristics of the depletion curve.

In the beginning of the ripening phase, the SCA starts decreasing a little on the western floor while landscape stays completely snow-covered on the eastern side. This remains for only a couple of days, from 1 to 8 June. On 25 June, the eastern floor overtakes the western one. The decline happens significantly faster on the eastern side than it does on the western side. From then on, the SCA constantly stays lower on the eastern side. This stands for differences in snow distribution and terrain roughness which deform the correlation of snow depth and SCA. Chapter 6.2.3 and the discussion (chapter 7) will take this topic on in further detail.

6.2.2 Particular snow cover depletion on the western slope

The SCA data also shows how snow cover decreases on the western slope. In comparison with the data from the valley floor the slope-SCA decreases almost linearly. The plot shows several minor spikes, which are related to changing weather conditions. The associated changes in image brightness result in adjusted thresholds in the analysis. The depletion of snow cover depends less on the contributing factors that were identified on the valley floor. Even the precipitation events do not arise in the slope data. The decrease in SCA starts on 17 May with 98%. At this point the snowpack on the valley floor is not isothermal by far and thus not ready for melting. This earlier start on the slope is due to differences in snow distribution, since a much higher energy input on the slope can be ruled out. For instance, the analysis of the snow-patch data shows that shortwave radiation is definitely lower on this slope.

The difference in local distribution of snow is studied extensively since it acts a part in modelling snowmelt runoff for hydrologic catchments. Pohl & Marsh (2006: 1775f) point out that Arctic environments show high rates in wind redistribution of snow because of their open and exposed landscape and their cold winters without freeze-melt-cycles that stabilise the snowpack. Snow is preferentially scoured from exposed locations such as slopes while deposition takes place as wind speed decreases in the lee of topographic features. In this case this results in a complex pattern of snow distribution where snow depth in average is low on the slope but gets trapped

in cracks and small lee areas where it melts successively. This again leads to a high small-scale variability in the depletion of the snow cover as it is shown in the next chapter (6.2.3) and the linear decrease in SCA. A similar but less pronounced effect is identified by Hinkler et al. (2002: 4680) for the mountainous part of their area of interest. They additionally point out that the snowmelt progresses from the valley floor to higher altitudes due to the temperature lapse rate. This is rather unlikely to be of importance here because the beginning of melting does not show a delay and further, the 50% SCA value is reached almost synchronously in all three areas. However, their research area has a much larger vertical extend.

6.2.3 Topography and small-scale variability of snow depletion

The time series of classified DCIs also allows to visualise the spatial pattern of snow depletion in the area of interest. Figure 15 shows the number of days each pixel is assigned to the snow class during the period of analysis. Since SCA decreases monotonic except a spike on 26 July, the figure's scale can be interpreted as the last day the respective pixel is snow covered. Accordingly, zero means snow-free from the first day of analysis on and 68 means snow covered throughout the whole period. Beginning is 17 May 2008 that is the 138th day of the year.

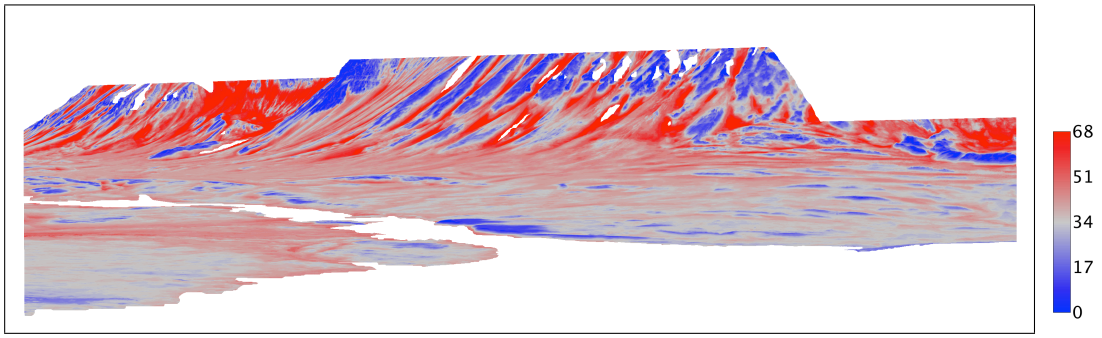

Figure 15: Small scale variability in the depletion of snow cover, shown as last day a pixel is snow covered. Scale is in number of snow covered days during the period of analysis. Blue colour represents regions of early melting while red indicates a late (or no) melting.

The figure (15) shows how the spatial pattern of snow depletion depends on topographical features. This is most notably pronounced on the western valley slope where melting is early on ridges with little snow depths and late (or never) in sinks and behind ridges where snow depths are higher due to the redistribution by wind. Some of the latter are avalanche run-outs where accumulation leads to higher snow depths. The variable surface results in the rather linear snow depletion curve here as described earlier (figure 12). The valley floor in general shows much less topographic features that are snow free early in the period. Here, most change happens in the

mid third of the analysis which results in a steep snow depletion curve and its S-shape (figure 12). The faster decrease in SCA on the eastern valley floor is also due to a rather even ground when compared to the western floor. The relation of snow depletion and topography is extensively studied by Schmidt et al. (2009). They show that the influence of topography on the snow cover pattern is high but that also other factors regarding the ground surface such as permafrost properties and vegetation cover have significant effect on the small scale snow depth.

Figure 15 shows a later melt-off on the western footslope than further in the valley centre. This is likely to be a consequence of wind redistribution of snow from the slope that accumulates here and leads to higher snow depths. Still, the eastern valley floor also shows a later depletion on its western side which is unlikely a result of winddrift. The DCI show evidence that this area of late melt-off shows congruence with the area that was flooded during the event on 28 May. According to the temperature sensors within the snowpack that are situated further south in the valley the snowpack was not yet isothermal at this point. This implies that at least some water from the flooding refreezes to the snow grains when the water that penetrates the snowpack is not significantly warmer than 0°C so that its sensible heat causes melting. The refrozen water naturally increases local SWE and hence, the time it takes the snow cover to clear away.

6.3 The postmelt period on the western slope

The snow-patch on the western valley slope is measured every other day during the phase after the main melt event. The dataset shows a fairly constant decrease in snow depth and size throughout two weeks. On 26 July, when the first complete set of values is available, the patch's size is 2299 m^2. The snow depth is 212.4 cm as the average of the five measurements on the snow-patch. Through the period of two weeks the snow-patch lost 54% in size as illustrated in figure 16 and 75 cm in thickness. Using the density of 393 $kg\,m^{-3}$ this equals a loss of 295 mm water equivalent. Compared to only 480 mm of annual precipitation, this impressively points out the importance of snow distribution to the ecosystem.

Figure 14 shows how the patch is exposed to direct solar radiation. As Schmidt (2007: 140) studies snow cover depletion, she concludes that this is of major relevance for spatial differences in snowmelt. Surrounding landscape covers a large part of the sun progression, resulting in a decreased shortwave radiation energy input. During 5:00 to 14:00 and 22:00 to 24:00, the solar shading allows approximately 11 of originally 24 hours of direct solar radiation onto the snow-patch. Actually, for 5:00 to 8:00 and 22:00 to 24:00, the sunlight comes in from less than 20° above the horizon and is therefore fairly weak. Additionally, the early morning would be the time with highest efficiency due to the exposure in east-north-eastern direction. Direct shortwave

Figure 16: Depletion of the measured snow-patch from 26 July (grey, 2299 m^2) to 9 August (white, 1243 m^2) as seen by the digital camera. Note that the shape is transformed by perspective bias.

radiation can therefore not contribute a large amount of energy for melting. However, diffuse solar radiation can still provide energy.

The 26th of July shows cloudy but bright conditions. The temperature of 6,4°C on the slope is relatively high and the presence of wind with an average of 5.5 $m\,s^{-1}$ promotes sensible heat fluxes. The clouds can act as diffuser for the shortwave radiation. This fits to the cloudy but bright-looking DCIs. The low clouds on the next day rather do not contribute a lot of energy via shortwave radiation but it is likely that they do so for longwave radiation. The loss in 17.4 cm snow depth for 26 and 27 July is the maximum for the period of measurements on the snow-patch.

The peak rate for loss in size arises with 654 m^2 from 28 to 30 July. On the 29th temperatures are up to 6.23°C high and there is also some precipitation involved. As temperature decreases down to 2.7°C on the next day, the high loss in size and the 14.2 cm depth decrease are likely caused by the high temperatures on the first day. This could indicate that melt is pretty much temperature driven at this point.

An increased amount of impurities on the snow surface is noticed on 30 July. This reduces albedo and therewith increases the effect of shortwave radiation. Since the measurements of snow depth are taken every other day the precise loss of depth or size is not available. Still, the data shows that ablation is relatively high for this day.

On 1 August a situation similar to 26 July occurs, where clouds increase the shortwave radiation input to the snow surface due to diffusion. The overcast conditions from 2 to 4 August with rather low temperature and wind speed again contribute only little to melting. The air with high humidity for these days can not contribute more than its sensible heat, since the snowpack is isothermal by far. Hence, the water does not freeze onto the snow grains and cannot liberate latent heat.

During the fieldwork, the surface of the inclined snow-patch now successively developed horizontal cracks. In addition, some creeping of the snowpack in downslope direction was noticed at the bottom of the snow-patch when doing the transect snow depth measurements along a fixed line. These two observations indicate that gravity forces caused deformations within the snowpack. Mechanical properties of snow are fairly complex. However, snow is a visco-plastic material that starts to creep as soon as a very small threshold stress is applied (Langham 1981: 299). Therefore, manipulation of the measurements due to snowpack transformation processes cannot be ruled out, especially because the surface showed respective evidence.

Overcast conditions and slow melting dominate the time from 5 to 9 August. Average air temperatures are rather low during these days as well as overall loss in snow-patch size and depth. Only the 5th shows clear sky conditions and probably a higher loss in size and snow depth. However, the coarse temporal resolution of measurements does not allow to recognise this in the data. Actually, this is the major problem that arises when analysing the depletion of the measured snow-patch. The discussion will go into further detail regarding the significance and usability of this data.

7 Discussion

The presented analysis is based on the relation of camera images, weather conditions and measurements in the field. Particularly the quality and significance of the image analysis method should be carefully considered. The following chapters assess the data quality and its explanatory power. Further, an outline of related changes in the context of Climate Change is given in chapter 7.4.

7.1 Method uncertainties and data quality

7.1.1 Evaluation of SCA data quality

The distinction between snow and bare ground to classify surface types in the images is based on the respective brightness in the DCIs. Figure 17 shows why the use of a individual threshold for every DCI is necessary. The scatterplot shows a of image brightness (of snow and bare ground, respectively) and the current SCA. With increasing SCA the whole image gets brighter because of the high reflectance of snow. This forces the camera in automatic mode to react with a shorter exposure time or a proper f-number, that both decrease image brightness and hence the brightness of snow and ground (Schmidt 2007). A smaller SCA value that means a higher

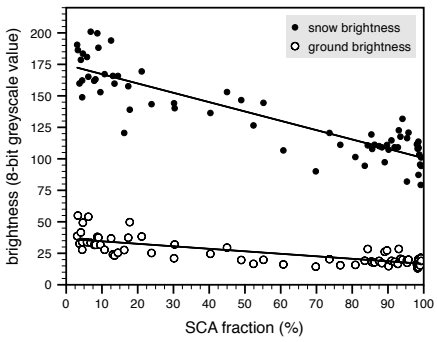

Figure 17: Relationship of the brightness of snow and bare ground to SCA fraction. Dots represent the images taken into account for the analysis ($n = 68$). Note that also weather conditions alter image brightness.

fraction of bare ground in the image section results in a lower overall image brightness and therefore a higher brightness of snow and ground. Altogether, figure 17 demonstrates that the threshold used for the surface type classification has to be adjusted to each image, because each DCI's brightness depends not only on weather conditions but also on SCA. Similar studies encounter the same challenge and apply different methods to find adequate thresholds or separation techniques. While Schmidt (2005, 2007) uses manually adjusted thresholds for different areas (regarding shadows from topography and bare ground brightness from geology), Hinkler et al. (2002) calculates an adapted index from coloured camera images.

Figure 17 indicates that the two classified surface types are not affected in the same strength by the described effect. The brightness of bare ground changes in the same direction as snow brightness changes but generally with lower intensity and some chaotic element in addition (e.g. weather conditions). As a result, the threshold's quality is higher when the brightness of both surfaces is used to establish a threshold value for the classification. In this work this is done by image standardisation to the two brightness values as it is described above (see e.g. figure 11).

Still, there remain questionable assumptions regarding the quality of the classification method. Since the brightness of single pixels varies widely it can never be ruled out that snow pixel are assigned to the "ground class" and vice versa in one single image. The proper way to respect this should be a detailed probabilistic approach that could e.g. use frequency distributions of the two classes to achieve a better individual threshold than just the center of brightness.

A problem that is rather reflected in the data is the representativeness of the two spots used to perform the measurements of the individual snow and ground brightness in all the DCIs. Since SCA is 99.3% (total area of interest) in the beginning of the time series there are only few spots to choose from for measuring the brightness of bare ground. Same holds for snow covered spots

in the end of the time series when SCA is only 4.1%. Figure 9 shows the location of the selected spots. Naturally, their respective brightness in the DCIs is not the universally valid value for all snow and ground surface in the image section. This is on the one side due to differences in the optical properties of the snow surface as they are seen by the digital camera. Potential factors are aeolian impurities on the snow surface as noticed on 30 July that can be related to surrounding terrain or the dependence of the optical properties e.g. on the angle of view (Gerland et al. 1999). On the other side, the large extend of the area of interest also allows partial shading by cloudcover. The SCA data for 26 July shows nicely how sensible this method is to such conditions where the spots for measuring snow and ground brightness are shaded by clouds (see figure 18). The brightness correction is then exaggerated resulting in an SCA output that is about 8.5% too high.

Figure 18: DCI on 26 July that shows partial shading by clouds which results in an exaggerated brightness correction

Since there is no reference data available for comparison, a direct quantitative approach to data failure ca not be given here. Still, the smoothness of the SCA plot (figure 12) shows that individual weather conditions are compensated by the method. Altogether, the SCA data quality can be rated good enough to allow the performed analysis. But the question now is whether the data is representative and how strong the transformation is by perspective bias.

7.1.2 SCA data representativeness and perspective bias

The data, which is obtained through analysis of the DCIs, is assumed to be representative for the whole Linnédalen catchment. Naturally, the DCI section only includes parts of the valley floor and the western slope. Especially in the southern part of the valley the topography becomes more complex and Linnébreen acts a part in the hydrological system. Since the image section is fixed, this is neglected in the analysis. The contributing conditions in this mesoscale area

should be homogenous enough to tolerate this issue, but including other areas in the investigation (particularly the eastern valley slope) would be interesting.

The analysis shows that studying the image sections separately is reasonable. The temporal decrease in SCA on the western slope is not very meaningful. If the raw aggregated data without the separation would be used, the slope data would flatten the depletion curve. Furthermore, this technique decreases the problem of perspective bias. The eastern valley floor is still situated in the image foreground, but the data for the different areas is not accumulated during analysis. Hence, the eastern floor as a whole is not overweighted. Still, inside the areas, there is some perspective bias, but it should not cause significant failures: Snow covered and snow free areas are both weighted higher in the foreground, as they would be in the background. This means that only if the SCA is heterogeneous within one of the three areas, the SCA in the foreground in this certain area is weighted higher than in the background. Additionally, the distance to the camera is already fairly large for the eastern valley floor area, which also decreases the perspective bias.

The camera's low angle of view causes some bias when the land surface is tilted. A tilt towards the camera lens causes a better exposure and therefore a higher weighting. On the valley floor, this is only the case on small scale, e.g. small ridges, where the face is weighted higher and backside is neglected since it is hidden or at least weighted lower. The slope as a whole shows this feature and therefore makes up a separate area in the analysis.

In similar studies, e.g. by Hinkler et al. (2002), Schmidt (2005, 2007) or Corripio (2004), respect to the perspective bias is given through orthographic rectification of the DCIs to produce orthophotos. This basically requires a high resolution digital elevation model as well as reference points in the field which both are not available here. Still, it would not only bypass perspective bias but would also allow to measure distances and areas in the DCIs. On the other hand, rectification requires further information to be precise e.g. about the camera's focal length and it can be questioned whether it would actually increase the information content of the method's results presented in this work and whether it would be worth the methodical effort. For comprehensive information on rectification and related methods see literature on photogrammetry or Corripio (2004) in the context of the presented method.

7.1.3 Data quality and relevance of the measurements on the snow-patch

Unfortunately, the largest part of the melting period was already over when the fieldwork started on 17 July and the measurements in the field were taken even later. Then, for logistical reasons, the measurements were taken every other day. This results in a total of only eight values each.

Difficulties in the analysis of the snow-patch's melting show that especially the temporal resolution is rather coarse for the analysis on this small scale. In addition, the accuracy of some results from this time span is questionable. As mentioned in the analysis part, motion of the snowpack may affect the snow depth values. Taking depth measurements not within one small area but distributed all over the snow-patch or along a transect could solve this problem. The latter was done in the field by gauging depth twice every meter along a horizontal 16 m transect. Processing the data of this transect could have provided reliable data for snow depth, but the track of originally 16 m melted down to 3 m length. This thwarts the idea of heaving multiple values to average and hence, the data is not taken into account.

For a reliable comparison with the SCA data, a representative value for snow depth on the same temporal resolution and the same timeframe would be helpful. Additionally, it should be representative for the whole camera's field of view. Goodison et al. (1981: 214) suggest to deploy stakes in the area of interest that have a coloured, vertical scale that is large enough to be read remotely – in this case from the camera's pictures. This would be a way of gaining spatial snow depth data through the whole season without a lot of effort. Christiansen (2001) shows that this approach works fine when the stakes are deployed in the vicinity of the camera (65–105 m). Naturally, the maximum distance is limited by camera image resolution and size of the graduation.

However, the first important progress would be to obtain data from the whole melting period. Especially some additional information about either the liquid water content or water output from the snowpack would help to make out the hydrological periods of melting precisely. To gain water equivalent values, density values are necessary as well, but as long as information about the actually released amount of water is unimportant it is only required to identify SCA-decrease due to compaction of the snowpack. In the runoff phase, where amounts of melted snow are interesting, the pore space holding capacity is reached anyway (Dingman 2002: 185–190) and density doesn't perform major changes. So, snow depth decrease correlates well with loss in water equivalent in this period.

7.2 Relationship of SCA, snow depth and water equivalent

The DCI analysis shows the temporal decline in snow covered area. In this investigation, mainly the influences of weather conditions on the SCA are studied. Obviously, there is a connection to the decline in water equivalent stored in the catchment as snow, but due to the terrain roughness SCA is not a linear function of water equivalent. Ferguson (1999: 210–212) shows this relationship between spatial variability in snow depth and melt rate and the temporal decline in SCA (figure 19).

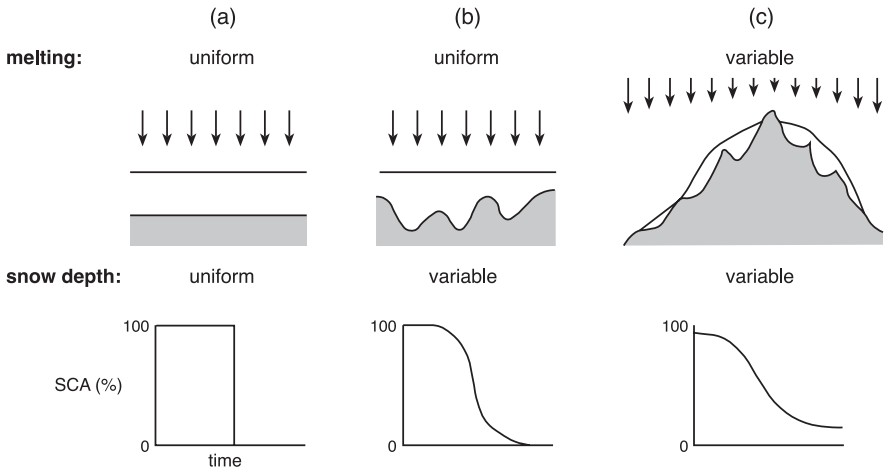

Figure 19: Relationship between spatial variability in snow dept, melt rate and decline in SCA (Ferguson 1999: 211).

Linnédalen can be seen as a combination of figure 19 (b) and (c) with a melt rate that is varies with time and location. The temporal variability is the major subject of this work. The spatial variability is due to differences in exposition to solar radiation and snow distribution. The figure (19) shows that already a uniform melt rate leads to a non-linear reduction of SCA on every natural terrain. This has to be taken into account, especially when referring to runoff. A fast decline in the SCA-plot does not directly equal a high loss in water equivalent and therefore peak discharge. However, this figure shows nicely where the S-shape in the SCA-plot comes from. As long as the above is kept in mind, the data from Linnédalen still offer a valuable proxy for analysing the melting period.

Davison & Pietroniro (2005: 2516) show snow depletion curves that can provide basin-specific information on the temporal decline in SCA. Figure 20 (a) shows a decrease in SCA for some

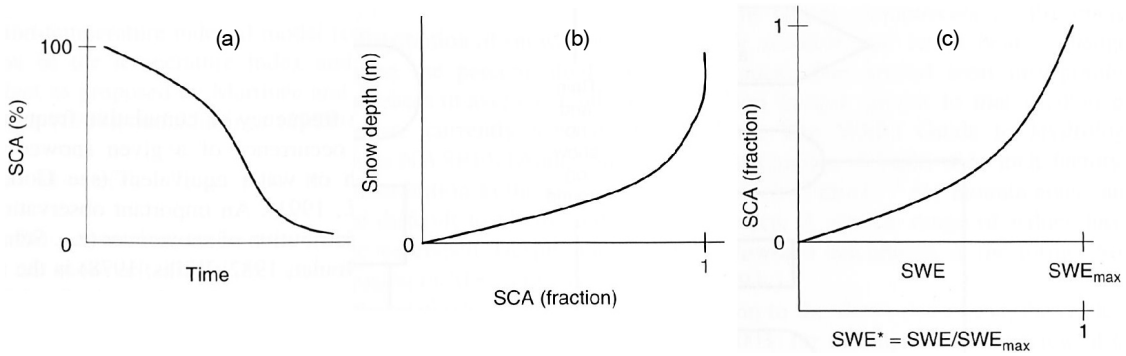

Figure 20: Relation of SCA and (a) time, (b) snow depth and (c) water equivalent (Davison & Pietroniro 2005: 2516).

exemplary spring plotted over time. This is in line with the findings in this investigation. However, this curve is not very meaningful regarding the basin-specific melting properties because it has the temporal variability of snow melt – e.g. due to weather conditions – aggregated in the data. Of further interest is the fact that snow cover tends to follow the same spatial pattern when in melts in every spring (Davison & Pietroniro 2005: 1516). Hence, snow depth decrease and SCA decrease follow a similar relation every spring. Figure 20 (b) shows how such a spatial, landscape specific correlation can look like. Figure 20 (c) is based on the same idea but shows the correlation of SCA and SWE instead.

These terrain specific properties show up nicely in the SCA data from Linnédalen. As mentioned above, the temporal decline in SCA happens differently on the western and the eastern valley floor. The eastern floor DCI section shows a more rapid decrease in SCA, tending a little to the graph in figure 19 (a). The western valley floor shows an earlier beginning in decrease which indicates that the land surface is rougher and has some points that poke out of the snow surface earlier. The latter is represented in the graphs (b) and (c) in figure 19 when neglecting the variability of the spatial snow distribution. This means that the area-specific relation of snow depth and SCA – as highlighted by Davison & Pietroniro (2005: 1516) – is different in the two areas. The graph in figure 20 (b) would be bent less for western valley floor and bent more for the eastern side. However, it could also be differences in the spatial distribution of snow that affect the character of melting on the valley floor but this cannot explain the faster decline in SCA on the eastern valley floor. An overlay of both factors cannot be ruled out since there is no spatial snow depth data available.

The ideal way of improving the explanatory power of the SCA data would be to obtain such area-specific information about the relation of SCA and overall snow depth. This would allow to make up at least for the non-linear correlation of snow depth and SCA. One scope of this work is to calibrate the SCA data in some way. Therefore, measurements of snow depth are taken among others in the field. They are taken into account in the analysis of the melting period. Still, it should be noted here that snow depth or SWE data generally is not of higher relevance than the SCA fraction. As shown in chapter 3.3, many important processes especially regarding vegetation are linked not only to snow depth and the amount of stored SWE but particularly to the presence and spatial extend of snow cover.

7.3 Similar studies in alpine and polar periglacial environments

As pointed out in the Introduction and Chapter 3.3, snow cover and its melting in Arctic ecosystems are studied extensively due to their importance for the biota and a wide range of physical processes. This work refers to various studies some of which use related methods to study the depletion and characteristics of snow cover.

7.3.1 Advantages using Digital Elevation Models and GIS for analysis

The common way to quantitatively analyse camera images of any terrain is to use reference points in the field for georeferencing the images. This allows to combine the images with a digital elevation model like done with terrestrial photographs by Aschenwald et al. (2001), Corripio (2004), Hinkler et al. (2002), Schmidt (2007) and others. As pointed out earlier, neither reference points in the field, nor a high resolution elevation model is available for the research area. Still, georeferencing the images can provide numerous advantages in the context of snow cover depletion analysis.

- The conversion to orthophotos avoids the perspective bias and allows setting of a scale (e.g. Hinkler et al. 2002).
- Georeferenced images can be laid over maps and elevation models. This allows to combine them with various other information such as height above sea level (e.g. in Hinkler et al. 2002: 4680) or vegegtion cover.
- When the images are used as raster type data in Geographical Information Systems (GIS) they allow to perform comprehensive statistical analysis such as done by Schmidt (2007) for topography and by Buus-Hinkler et al. (2006) for the effect on vegetation cover.

The latter is an especially interesting approach since GIS analysis can respect variations in relief, exposure, aspect and shading by topography (Corripio 2004; Schmidt 2007 and others). Additionally, it allows to include data from other sources such as remote sensing. This is done by Buus-Hinkler et al. (2006) as they study the relation of snow cover and vegetation in the Zackenberg area, Greenland. The satellite data allows them to apply their modelling results derived from DCI analysis to years prior to the installation of the camera.

7.3.2 Enhanced method results by using additional spectral bands and remote sensing

In the presented method surface type classification is based on greyscale brightness of each pixel. Hinkler et al. (2002) presents a way to calculate a snow classification index that is based on the red, green and blue values (RGB) from standard digital camera images. This index corresponds to the "Normalized Difference Snow Index" (NDSI) that is widely used to analyse Landsat Thematic Mapper and other satellite images. The standard NDSI is calculated as shown in formula 5 with VIS as the visible and IR_{mid} as the mid-infrared spectral band (Hinkler et al. 2002: 4674). It is based on the spectral reflectance of snow that rapidly decreases in the infrared band of the spectrum.

$$NDSI = \frac{VIS - IR_{mid}}{VIS + IR_{mid}} \tag{5}$$

Hinkler et al. (2002) empirically found relationships between the three colour channels (RGB) that are typical for snow surfaces while being independent on illumination intensity. They use these relationships to calculate a replacement for the IR_{mid} part in the NDSI formula. The outcome is a related index that is independent from image brightness and also partial shading of the image section by cloud cover or surrounding topography (Hinkler et al. 2002: 4673–4675). Unfortunately, this promising method could not be applied here. Using IDRISI to perform the calculations did not result in reasonable results. This was likely due to 1) a different camera type with different internal filters and – rather important – 2) division of large values by close-to-zero for some pixels. The latter might be a problem of the used camera, its processing algorithms or even data compression. Schmidt (2007) also tries to apply this index to her images but finds that it is not capable of separating shaded snow from light-coloured rock in her research area.

Another study that uses the three colour channels (RGB) of terrestrial camera images is given by Svensson (2005), who calculates a "Greenness Index" to gain information about vegetative activity in northern Sweden. Still, she encounters problems to separate vegetation from snow with a fixed threshold due to varying image brightness (Svensson 2005: 15f). When Buus-Hinkler et al. (2006) study vegetative activity in the Zackenberg area, Greenland, they also use terrestrial but multispectral photography to calculate the standard "Normalized Difference Vegetation Index" using the actual near-infrared spectral band (Buus-Hinkler et al. 2006: 239f).

Remote sensing methods can be used to gain numerous data about the snowpack, including water equivalent and snow depth. Koenig et al. (2001: 10–12) give an overview about remote sensing of snow and glacier ice. They show that the microwave region allows mapping of water

equivalent since it penetrates into the snowpack. The disadvantage of using satellite data is not only the spatial, but also the temporal resolution, which varies widely from less than a day to several weeks. Usually high temporal resolution data is available with only low spatial and vice versa (Schmidt et al. 2009). Additionally, the optical properties of snow are complex and change with time. This makes it difficult to distinguish between snow and clouds in some bands and between snow and bare land surface in other bands. The method presented in this work can not offer the same sophisticated data, but still provides useful information on a high spatial and temporal resolution. Altogether it can be concluded that remote sensing could contribute relevant information to the presented results, like done by Buus-Hinkler et al. (2006), but can not be seen as a substitute for it.

7.4 High Arctic snow cover – complex linkage to a changing climate

As highlighted in chapter 3.3 the melting of snow and sea ice cover strongly interacts with Climate Change. This work shows that timing and spatial characteristics of snowmelt depend on a wide range of factors that provide an even wider range of interactions with changing climatic conditions. Although air temperature is a major driving force on snowmelt, a closer look on some of the relevant factors will show that the influences by a changing climate are highly complex.

First of all, the duration of snow cover in spring is determined by the end of winter snowpack thickness and therewith by the amount of winter precipitation. Model projections are used to quantify possible changes in precipitation based on different future emission scenarios (Meehl et al. 2007). With respect to the Arctic, detailed model results are e.g. provided by the Arctic Climate Impact Assessment (Kattsov et al. 2005). Their five-model mean suggests an 12.3% increase in annual precipitation north of 60° N with greatest increase in autumn and winter (Kattsov et al. 2005: 125,127). This is generally in line with recent observations – also on Svalbard (e.g. Førland & Hanssen-Bauer 2000: 496). Although this indicates a general increase in snow, the effect is encountered by rising temperatures. Førland & Hanssen-Bauer (2000: 496) show for Ny-Ålesund that during the period 1964–1997 the fraction of mainly mixed (sleet) but also liquid (rain) precipitation increased at the expanse of a reduce in snow type precipitation fraction of 5.8% per decade. The balance of increasing precipitation on the one side and higher temperatures on the other side determines whether snow will be increased or reduced (Räisänen 2008: 307). This makes it particularly difficult to estimate snowfall in a future climate but can lead to an increase in regions that remain consistently below freezing (Walsh et al. 2005: 199). For a detailed interpretation of climate model projections on future snowfall and SWE see Räisänen (2008). Regarding Svalbard, his model mean shows a slight increase in snowfall (0–15%) for the late

21st century. Still, a reduce of seasonal snow cover extent and duration is a widespread and robust feature in model projections – for the Subarctic but also for some regions where amounts of snowfall increase (Räisänen 2008; Walsh et al. 2005; Meehl et al. 2007: 770).

Although the snow cover reduction on the global scale is largely determined by rising temperatures and changed precipitation characteristics many other factors need to be considered when referring to the melting process. The analysis showed that the special radiation properties of snow determine some important energy fluxes to the snowpack. As highlighted by Zhang et al. (1996: 2122) a possibly higher degree in cloud cover in the context of Climate Change would lead to extra longwave radiation and contribute to a positive net energy balance of snow cover. This would in turn support the big positive feedback loop induced by melting and the subsequent albedo change (Zhang et al. 1996: 2122). However, the reaction of cloud cover to Climate Change is highly complex. As pointed out by Kattsov et al. (2005: 116f), cloud cover and especially its physical characteristics are still difficult to model. Since the effect of clouds on the snow energy balance heavily depends on the cloud characteristics such as thickness, height, temperature and particle size, the future impact on snowmelt can hardly be quantified. For instance, low and thin clouds generally cause a more positive energy balance than high or thick clouds (Zhang et al. 1996: 2121f). Furthermore, anthropogenic emissions could provide additional freezing nuclei in the atmosphere, changing precipitation characteristics but also drop size of clouds that determines radiation characteristics (Zhang et al. 1996: 2121f). At the same time, the impact of clouds on the snow energy balance also depends on the optical properties of the snow cover: when snow albedo is low in the late melting season the reduce in shortwave radiation by clouds counteracts the increased longwave radiation (Zhang et al. 1996: 2121f). Altogether, this means that assessing the effect of future cloud cover requires comprehensive knowledge on changes in cloud characteristics and their seasonal cycle.

In the analysis many more atmospherical processes are found to alter the net energy balance of snow and therewith its warming and melting rates that are all in some manner related to atmospheric circulation. One group is identified as turbulent heat fluxes comprising not only sensible heat as air temperature but also sensible and latent heat from precipitation. Recent climate change research has shown that precipitation and temperature will not only change their mean seasonal behaviour but also their character of occurrence: generally, the frequency and intensity of extreme events will very likely increase (e.g. Meehl et al. 2007). In the context of snowmelt, this could result in a higher probability of mild and wet conditions during winter. This again can lead to partial melting and also to the forming of ice layers within the snowpack that e.g. hinder the accessibility of food for reindeer (Solberg et al. 2001). The intensity of some turbulent heat fluxes to the snow surface also depends on the atmospheric mixture by wind, which

is another variable to consider. Walsh et al. (2005: 201) point out that especially in the context of blowing snow, sublimation as a part of the hydrological cycle is a "potentially important but often overlooked process" and naturally influences late winter amounts of snow.

So far, emphasis was put on changes in atmospherical processes, but Climate Change will also affect the terrestrial ecosystem with indirect relation to the snow cover. An issue that is widely neglected in this work is the relation of snow cover and vegetation, because the High Arctic research area on Svalbard does not allow growing of relevant species such as shrubs – in present day climate. Sturm et al. (2005: 1f) show that shrubs not only reduce snow redistribution but that they significantly alter surface albedo in winter. Measuring radiation on various sites in Alaska they find that a transition from shrub-free to shrubland can increase winter heating by up to 70% (Sturm et al. 2005: 1f). This exemplary shows that the effect of future changes in vegetation cover must not be undervalued, although it seems far from the present situation on Svalbard. However, some subarctic regions such as Alaska evidently experience the described increase in shrub abundance (Sturm et al. 2005: 1).

All of the mentioned processes could in turn support the big positive feedback cycle when increased melting of snow leads to a lower land surface albedo and therewith to further warming. However, French (2007: 381f) points out that this not necessarily holds for regions that will experience more snow and a higher albedo which could dampen the Climate Change. Still, in many cases the sign of trend is obvious. For Svalbard this is e.g. reflected by the fractional decrease in snow type precipitation found by Førland & Hanssen-Bauer (2000: 496). But identification of climatic trends is difficult because they are overlain by the natural variability. Winther et al. (2002: 132) can make out a slight trend towards increased melt rates in Ny-Ålesund for the period 1981–1997 but there are no clear trends in snow arrival and melt timing. They conclude that this could be due to the short time period that was investigated (Winther et al. 2002: 138) and furthermore, model projections agree on the prevailing effect of rising temperature – although they show significant deficiencies in reproducing the complex interaction of snow cover, its melting and a changing climate (Walsh et al. 2005; Randall et al. 2007).

The high vulnerability of the Arctic to global Climate Change arises all over the ecosystem. Chapter 3.3 shows the drastic importance of snow melt timing and snow cover characteristics to the hydrological system, to geomorphology and also flora and fauna. As long as there remain the described uncertainties in the knowledge on relevant processes and feedback cycles a quantitative assessment on climate change impact on the Arctic ecosystem can not be given, particularly not on local scale – such as the Linnédalen catchment.

8 Conclusions

The presence of snow cover and the timing of its melting are of drastic importance to High Arctic ecosystems. They determine the length of the growing season and the availability of liquid water, affecting flora and fauna. Furthermore, a wide range of geomorphological processes depend not only on the presence of meltwater but especially on frost-thaw cycles that are limited by the insulating character of the snowpack. Snow determines surface albedo and has a high sensitivity to rising temperatures. This drives the probably best-known feedback cycle for Climate Change and makes the Arctic exceptionally vulnerable to increasing temperatures. Altogether, this indicates the importance of a comprehensive knowledge on the melting characteristics of snow cover, especially on the background of a changing climate.

From the hydrological point of view the melting period can be separated into the warming phase which is characterised by the increase in snow temperature until the whole snowpack is isothermal at the melting point. During the ripening phase the pore spaces between snow grains get filled up with liquid water and finally water output happens during the runoff phase. In this investigation, this separation is followed in a dataset of snow covered area for the research area in Linnédalen in western Spitsbergen, Svalbard. The data is obtained from processing standard digital camera images by applying a greyscale threshold filter on the images after standardising their brightness. The outcome is a set of binary type images that allow to calculate the snow covered area fraction with respect to different regions within the image section. In combination with meteorological data from a weather station, albedo, snowpack temperature and a couple of fieldwork measurements the dataset provides a comprehensive record on the behaviour of spring snowmelt on a remarkably high temporal and spatial resolution.

The High Arctic research area ensures a clear definition of winter and the melting period that is not disturbed by major snowfall events. In the late winter, just before the melting period begins, fractional snow cover on the Linnédalen bottom and the lower valley slope is close to 100%. In spring 2008 snowpack temperatures start increasing in late April and the isothermal state is reached on 31 May. From this point on melting occurs and the snow covered area fraction decreases. The free water within the snowpack affects albedo which allows to conclude from the data that the pore spaces are filled up on 6 June. Afterwards, additional energy input produces meltwater runoff. However, melting is non-uniform within Linnédalen and the following factors are found to determine the spatial variability of snowmelt on the local scale:

- While winter precipitation controls the initial snowfall the actual spatial distribution of snow is largely determined by wind. Snow is redistributed during the cold season with

erosion at exposed spots and accumulation on the lower valley slopes or in the lee of topographic features. This leads to a non-uniform distribution of snow cover when the melting period begins.

- A number of factors that can be grouped as "topoclimate" determine the strength of energy fluxes to the snow surface. This comprises aspect, inclination and shading by surrounding topography.
- Local events can significantly alter the spatial depletion of snow cover. In the Linnédalen data these are 1) small avalanches on the western valley slope that efficiently redistribute snow and 2) a flooding event on 28 May in parts of the eastern valley floor, possibly from Kongressvatnet. Some of the water refroze in the snowpack ($< 0°C$) which increases the local snow water equivalent and thereby delays snow depletion.

The described processes lead to the non-uniform distribution and depletion of snow cover as it is reflected in the data on snow covered area showing a S-shaped graph. This is generally in line with similar studies. The daily variability of melting rates or rather the loss in snow covered area depends on the following factors:

- Naturally, the weather conditions drastically determine the energy fluxes on the snowpack. This is mainly air temperature as sensible heat, precipitation as latent and sensible heat, wind, shortwave and longwave radiation. The latter largely depends on cloudiness since clouds can reduce shortwave and increase longwave radiation.
- The snowpack characteristics such as grain size, density, stratigraphy and albedo determine its sensibility to the various energy fluxes. Albedo is exceptionally important since it controls the absorption of global radiation.
- As soon as the snow covered area fraction decreases and snow cover becomes patchy the local advection of sensible heat starts driving a positive feedback. Warm air from snow-free spots with low albedo supports melting of surrounding snow-patches when wind is present.

Precipitation as well as the interaction of albedo and cloud cover are particularly interesting. In the early melting season albedo is very high (> 0.8). This makes shortwave radiation an inefficient source of energy and underlines the importance of longwave radiation by cloud cover. Since air temperature is still low at this point this suggests that the onset of melting is largely influenced by cloud cover and additional energy input from rain that releases latent heat when freezing within the snowpack. In the late season when albedo is low (< 0.4) the cloud cover has a less positive effect on the snow energy balance and rain does not liberate latent heat when falling

on a snowpack in isothermal state. Therewith the sensibility to the respective energy sources changes as the melting progresses.

The results obtained by analysing camera images provide information on snow covered area which is significantly different from data on snow water equivalent or snow depth as they are measured e.g. by remote sensing methods. Since there is no data on the actual loss in water equivalent on runoff available a numerical assessment of the hydrological impact can not be given in this work. However, the ecological relevance of snow cover is particularly given by its insulating character and hence its spatial extend which is covered by the used method. In similar studies using terrestrial photography (e.g. Hinkler et al. 2002; Schmidt 2007; Svensson 2005) georeferenced images are used in combination with digital elevation models or further information what allows a statistical analysis of the spatial behaviour of snowmelt. In contrast to remote sensing methods the given results provide a less sophisticated but still meaningful dataset on a higher temporal and spatial resolution.

This work contributes to a detailed image of the spring snowmelt in Linnédalen with special emphasis on factors controlling the temporal and spatial variability of snow depletion. Its motivation is due to the drastic importance of snow cover characteristics and timing for the High Arctic ecosystem. The strong linkage to climatic conditions make snow cover exceptionally vulnerable to Climate Change. As long as present day processes are not fully understood the prediction of future changes in snow cover characteristics and timing is prone to large uncertainties. Although there remain major questions such as the future impact of cloud cover on snowmelt or vegetation on winter surface albedo, the trend towards a decrease in seasonal snow cover is evident. Ecologic relations are highly complex but due to its insulating character and hydrological importance the changes in snow cover will for sure have drastic consequences to Arctic geomorphology and biota.

Acknowledgements

The fieldwork in 2008 in Linnédalen was part of the course on “Holocene and Modern Climate Change in the High Arctic, Svalbard” at the University Centre in Svalbard (UNIS) in collaboration with the Research Experience for Undergraduates (REU) programme by the US National Science Foundation. The author wishes to thank UNIS and the REU programme for the support in materials and logistics and the possibility to work on the data that was collected in this context.

Further, thanks to Hanne Christiansen for advice and recent support and to the students and associates for their helpful work, ideas and discussions in the field.

References

American Avalanche Association (2010). *Snow, Weather and Avalanches: Observational Guidelines for Avalanche Programs in the United States*. USDA Forest Service National Avalanche Center, Pagosa Springs.

Anisimov, O. A., Vaughan, D. G., Callaghan, T. V., Furgal, C., Marchant, H., Prowse, T. D., Vilhjálmsson, H. & Walsh, J. E. (2007). Polar regions (Arctic and Antarctic). In *Climate Change 2007: Impacts, Adaptation and Vulnerability. Contribution of Working Group II to the Fourth Assessment Report of the Intergovernmental Panel on Climate Change* (pp. 653–685). Cambridge University Press, Cambridge.

Aschenwald, J., Leichter, K., Tasser, E. & Tappeiner, U. (2001). Spatio-temporal landscape analysis in mountainous terrain by means of small format photography: a methodological approach. *IEEE Transactions on Geoscience and Remote Sensing*, 39(4), 885–893.

Blümel, W. (1999). *Physische Geographie der Polargebiete*. Teubner, Stuttgart.

Bore, R. R., Andreassen, I., Kristiansen, J. E. & Mellemstrand, C. (2009). *This is Svalbard. What the figures say.* Statistics Norway, Oslo.

Brown, R. & Armstrong, R. L. (2008). Snow-cover data: measurement, products and sources. In R. L. Armstrong & E. Brun (Eds.), *Snow and Climate: Physical Processes, Surface Energy Exchange and Modeling* (pp. 181–216). Cambridge University Press, Cambridge.

Buus-Hinkler, J., Hansen, B. U., Tamstorf, M. P. & Pedersen, S. B. (2006). Snow-vegetation relations in a High Arctic ecosystem: Inter-annual variability inferred from new monitoring and modeling concepts. *Remote Sensing of Environment*, 105(3), 237–247.

Christiansen, H. H. (2001). Snow-cover depth, distribution and duration data from northeast Greenland obtained by continuous automatic digital photography. *Annals of Glaciology*, 32(1), 102–108.

Christiansen, H. H. (2004). Meteorological control on interannual spatial and temporal variations in snow cover and ground thawing in two northeast Greenlandic Circumpolar-Active-Layer-Monitoring (CALM) sites. *Permafrost and Periglacial Processes*, 15(2), 155–169.

Collins, T. J. (2007). ImageJ for microscopy. *Biotechniques*, 43(Supp. 1), 25–30.

Corripio, J. G. (2004). Snow surface albedo estimation using terrestrial photography. *International Journal of Remote Sensing*, 25(24), 5705–5729.

Davison, B. & Pietroniro, A. (2005). Hydrology of Snowcovered Basins. In M. G. Anderson (Ed.), *Encyclopedia of Hydrological Sciences* (pp. 2505–2532). John Wiley & Sons, Chichester.

Dingman, S. L. (2002). *Physical Hydrology*. Prentice-Hall, New Jersey.

Ferguson, R. I. (1999). Snowmelt runoff models. *Progress in Physical Geography*, 23(2), 205–227.

Flassak, T. (2007). *Sun's location / Sonnenstand*. Landeshauptstadt Stuttgart, Amt für Umweltschutz, Abt. Stadtklimatologie: http://cgi.stadtklima-stuttgart.de/mirror/sonnefre.exe (8.7.2010).

Førland, E. J. & Hanssen-Bauer, I. (2000). Increased precipitation in the Norwegian Arctic: true or false? *Climatic Change*, 46, 485–509.

French, H. M. (2007). *The periglacial environment*. John Wiley & Sons, Chichester.

Gerland, S., Winther, J. G., Ørbæk, J. B., Liston, G. E., Øritsland, N. A., Blanco, A. & Ivanov, B. (1999). Physical and optical properties of snow covering Arctic tundra on Svalbard. *Hydrological Processes*, 13(14-15), 2331–2343.

Goodison, B. E., Ferguson, H. L. & McKay, G. A. (1981). Measurement and data analysis. In D. M. Gray & D. H. Male (Eds.), *Handbook of Snow: Principles, Processes, Management and Use* (pp. 191–274). Pergamon Press, Toronto.

Gray, D. M. & Male, D. H. (1981). Snowcover Ablation and Runoff. In D. M. Gray & D. H. Male (Eds.), *Handbook of Snow: Principles, Processes, Management and Use* (pp. 360–436). Pergamon Press, Toronto.

Gray, D. M. & Prowse, T. D. (1993). Snow and floating ice. In D. R. Maidment (Ed.), *Handbook of Hydrology*. McGraw-Hill Professional, New York.

Hinkler, J., Ørbæk, J. B. & Hansen, B. U. (2003). Detection of spatial, temporal, and spectral surface changes in the Ny-Ålesund area 79 ° N, Svalbard, using a low cost multispectral camera in combination with spectroradiometer measurements. *Physics and Chemistry of the Earth, Parts A/B/C*, 28(28–32), 1229–1239.

Hinkler, J., Pedersen, S. B., Rasch, M. & Hansen, B. U. (2002). Automatic snow cover monitoring at high temporal and spatial resolution, using images taken by a standard digital camera. *International Journal of Remote Sensing*, 23(21), 4669–4682.

Hock, R. (2005). Glacier melt: a review of processes and their modelling. *Progress in Physical Geography*, 29(3), 362–391.

Humlum, O., Instanes, A. & Sollid, J. L. (2006). Permafrost in Svalbard: a review of research history, climatic background and engineering challenges. *Polar Research*, 22(2), 191–215.

Kattsov, V. M., Källén, E., Cattle, H., Christensen, J., Drange, H., Hanssen-Bauer, I., Jóhannesen, T., Karol, I., Räisänen, J., Svensson, G. & Vavulin, S. (2005). Future climate change: modeling and scenarios for the Arctic. In *Arctic Climate Impact Assessment* (pp. 99–150). Cambridge University Press, Cambridge.

King, J. C., Pomeroy, J. W., Gray, D. M., Fierz, C., Föhn, P. M. B., Harding, R. J., Jordan, R. E., Martin, E. & Plüss, C. (2008). Snow–atmosphere energy and mass balance. In R. L. Armstrong & E. Brun (Eds.), *Snow and Climate: Physical Processes, Surface Energy Exchange and Modeling* (pp. 70–124). Cambridge University Press, Cambridge.

Koenig, M., Winther, J. G. & Isaksson, E. (2001). Measuring snow and glacier ice properties from satellite. *Reviews of Geophysics*, 39(1), 1–27.

Langham, E. J. (1981). Physics and Properties of Snowcover. In D. M. Gray & D. H. Male (Eds.), *Handbook of Snow: Principles, Processes, Management and Use* (pp. 275–337). Pergamon Press, Toronto.

Liston, G. E. (1995). Local advection of momentum, heat, and moisture during the melt of patchy snow covers. *Journal of Applied Meteorology*, 34(7), 1705–1715.

Liston, G. E. (1999). Interrelationships among Snow Distribution, Snowmelt, and Snow Cover Depletion: Implications for Atmospheric, Hydrologic, and Ecologic Modeling. *Journal of Applied Meteorology*, 38(10), 1474–1486.

Marsh, P. (1999). Snowcover formation and melt: recent advances and future prospects. *Hydrological Processes*, 13(14–15), 2117–2134.

McClung, D. & Schaerer, P. (2006). *The Avalanche Handbook*. The Mountaineers Books, Seattle.

Meehl, G. A., Stocker, T. F., Collins, W. D., Friedlingstein, P., Gaye, A. T., Gregory, J. M., Kitoh, A., Knutti, R., Murphy, J. M., Noda, A., Raper, S. C. B., Watterson, I. G., Weaver, A. J. & Zhao, Z.-C. (2007). Global Climate Projections. In *Climate Change 2007: The Physical Science Basis. Contribution of Working Group I to the Fourth Assessment Report of the Intergovernmental Panel on Climate Change* (pp. 747–845). Cambridge University Press, Cambridge.

Neumann, N. & Marsh, P. (1998). Local advection of sensible heat in the snowmelt landscape of Arctic tundra. *Hydrological Processes*, 12(10–11), 1547–1560.

Norsk Polarinstitutt (2008). *Nordenskiöld Land, Spitsbergen. Turkart Svalbard 1 : 200 000*. Norsk Polarinstitutt, Tromsø.

Norsk Polarinstitutt (2010). *Svalbardkartet (http://www.npolar.no/svalbardkartet/, 5.7.2010)*. Norsk Polarinstitutt, Tromsø.

Norwegian Meteorological Institute (2010). *eKlima*. http://eklima.met.no (30.6.2010).

Pohl, S. & Marsh, P. (2006). Modelling the spatial-temporal variability of spring snowmelt in an arctic catchment. *Hydrological Processes*, 20(8), 1773–1792.

Pomeroy, J. W., Marsh, P. & Gray, D. M. (1997). Application of a distributed blowing snow model to the Arctic. *Hydrological Processes*, 11(11), 1451–1464.

Räisänen, J. (2008). Warmer climate: less or more snow? *Climate Dynamics*, 30(2-3), 307–319.

Randall, D. A., Wood, R. A., Bony, S., Colman, R., Fichefet, T., Fyfe, J., Kattsov, V., Pitman, A., Shukla, J., Srinivasan, J., Stouffer, R. J., Sumi, A. & Taylor, K. E. (2007). Cilmate Models and Their Evaluation. In *Climate Change 2007: The Physical Science Basis. Contribution of Working Group I to the Fourth Assessment Report of the Intergovernmental Panel on Climate Change* (pp. 589–662). Cambridge University Press, Cambridge.

Schmidt, S. (2005). Untersuchungen zur räumlichen und zeitlichen Verteilung der saisonalen Schneedecke in Abhängigkeit zum Relief mittels terrestrischer Digitalaufnahmen im Lötschental (Wallis). *Berliner Geographische Arbeiten*, 100, 29–35.

Schmidt, S. (2007). *Die reliefabhängige Schneedeckenverteilung im Hochgebirge - ein multiskaliger Methodenverbund am Beispiel des Lötschentals (Schweiz)*. Dissertation, Mathematisch-Naturwissenschaftlichen Fakultät, Universität Bonn.

Schmidt, S., Weber, B. & Winiger, M. (2009). Analyses of seasonal snow disappearance in an alpine valley from micro-to meso-scale (Loetschental, Switzerland). *Hydrological Processes*, 23(7), 1041–1051.

Solberg, E. J., Jordhøy, P., Strand, O., Aanes, R., Loison, A., Sæther, B. & Linnell, J. D. C. (2001). Effects of density-dependence and climate on the dynamics of a Svalbard reindeer population. *Ecography*, 24(4), 441–451.

Stone, R., Dutton, E., Harris, J. & Longenecker, D. (2002). Earlier spring snowmelt in northern Alaska as an indicator of climate change. *Journal of Geophysical Research*, 107(D10), 4089.

Sturm, M., Douglas, T., Racine, C. & Liston, G. (2005). Changing snow and shrub conditions affect albedo with global implications. *Journal of Geophysical Research*, 110, G01004.

Svensson, S. (2005). *Snow cover dynamics and plant phenology documentation using digital camera images and their relation with CO2-fluxes at Stordalen mire, Northern Sweden*. Degree-thesis, Department of Physical Geography and Ecosystems Analysis, Lund University.

Walsh, J. E., Anisimov, O., Hagen, J. O. M., Jakobsson, T., Oerlemans, J., Prowse, T. D., Romanovsky, V., Savelieva, N., Serreze, M., Shiklomanov, I. & Solomon, S. (2005). Cryosphere and hydrology. In *Arctic Climate Impact Assessment* (pp. 183–242). Cambridge University Press, Cambridge.

Winther, J. G., Gerland, S., Ørbæk, J. B., Ivanov, B., Blanco, A. & Boike, J. (1999). Spectral reflectance of melting snow in a high Arctic watershed on Svalbard: some implications for optical satellite remote sensing studies. *Hydrological Processes*, 13(12–13), 2033–2049.

Winther, J. G., Godtliebsen, F., Gerland, S. & Isachsen, P. E. (2002). Surface albedo in Ny-Ålesund, Svalbard: variability and trends during 1981-1997. *Global and Planetary Change*, 32(2–3), 127–139.

Zhang, T., Stamnes, K. & Bowling, S. A. (1996). Impact of Clouds on Surface Radiative Fluxes and Snowmelt In the Arctic and Subarctic. *Journal of Climate*, 9(9), 2110–2123.

Appendices

Table A-1: The main results: weather station data, brightness of snow and bare ground and SCA fraction data. Missing values are due to weather conditions.

	weather station				image analysis					
	Precipitation (mm·day^{-1})	Windspeed avg. (m·s^{-1})	Albedo (%)	Temperature (°C)	Snow brightness (0–255)	Soil brightness (0–255)	SCA total area o. i. (%)	SCA western floor (%)	SCA eastern floor (%)	SCA western slope (%)
17.05.08	0	1.40	0.85	-2.01	94.36	18.92	99.27	99.59	100.00	98.11
18.05.08	0	2.90	0.85	-2.18	95.43	15.39	98.98	99.52	100.00	97.18
19.05.08	0	1.57	0.84	-3.15	103.38	17.06	98.76	99.51	100.00	96.35
20.05.08	0	1.33	0.83	-3.14	79.27	21.50	99.16	99.71	100.00	97.46
21.05.08	0	4.26	0.81	-2.04	113.68	15.64	98.51	99.46	100.00	95.52
22.05.08	0	3.71	0.83	-0.83	108.03	13.06	98.28	99.46	100.00	94.66
23.05.08	0.2	3.28	0.81	0.00	108.46	20.32	98.50	99.48	100.00	95.45
24.05.08	0	0.78	0.81	-0.67	87.24	13.86	98.53	99.38	100.00	95.75
25.05.08	0	1.95	0.78	0.64	101.08	21.03	99.26	99.39	100.00	98.50
26.05.08	2	2.71	0.77	0.60	111.43	16.15	98.08	99.19	100.00	94.49
27.05.08	0.2	0.79	0.79	0.64	108.92	18.96	98.52	99.35	100.00	95.80
28.05.08	0	2.51	0.76	1.14	111.96	17.30	98.24	99.14	100.00	95.17
29.05.08	0	2.45	0.76	-0.04	-	-	-	-	-	-
30.05.08	0	4.98	0.73	1.58	-	-	-	-	-	-
31.05.08	0	4.72	0.69	2.20	-	-	-	-	-	-
01.06.08	0.6	3.09	0.62	2.44	-	-	-	-	-	-
02.06.08	6.6	3.81	0.54	2.04	-	-	-	-	-	-
03.06.08	0.2	5.84	0.62	1.07	120.80	19.94	95.74	97.46	99.89	89.36
04.06.08	0	0.92	0.72	1.51	116.41	17.44	95.35	97.60	100.00	87.53
05.06.08	0	0.89	0.71	1.67	81.94	19.55	95.30	97.37	100.00	87.81
06.06.08	0	1.62	0.54	0.17	131.76	19.94	94.06	96.95	99.94	84.07
07.06.08	0	0.80	0.53	1.46	117.58	20.58	93.48	96.53	99.89	82.80
08.06.08	0	0.98	0.53	1.12	109.13	16.56	92.77	96.07	99.86	81.12
09.06.08	0	1.14	0.46	1.63	122.64	28.41	93.03	96.01	99.81	82.24
10.06.08	0	2.78	0.42	2.07	109.18	18.14	91.84	95.38	99.69	79.16
11.06.08	0.2	4.36	0.38	1.70	114.65	19.02	90.97	95.04	99.57	76.69
12.06.08	0	3.36	0.37	1.80	107.25	14.77	90.17	94.23	99.14	75.65
13.06.08	0	6.32	0.34	1.58	111.03	27.26	89.73	93.47	98.59	75.94
14.06.08	0	4.44	0.33	1.21	109.12	17.20	88.31	92.96	98.07	72.01
15.06.08	0	8.19	0.33	0.45	97.29	26.18	89.08	92.97	97.57	75.27

continued

Table A-1: *continued*

	Precip.	Windsp.	Albedo	Temp.	Snow br.	Soil br.	SCA total	SCA west	SCA east	SCA slope
16.06.08	0	3.61	0.34	0.74	110.09	18.96	87.51	92.23	97.30	71.08
17.06.08	0	2.28	0.32	0.45	111.19	17.80	86.24	91.10	96.71	69.06
18.06.08	0	2.93	0.31	0.72	107.82	17.89	85.59	90.64	96.49	67.70
19.06.08	0	2.61	0.29	1.53	119.34	18.53	85.36	90.34	96.06	67.78
20.06.08	0	2.02	0.29	1.56	110.69	28.39	84.34	89.56	95.28	66.07
21.06.08	0	0.84	0.36	3.38	94.46	19.09	83.50	88.55	94.23	65.75
22.06.08	13.2	3.48	0.20	3.01	-	-	-	-	-	-
23.06.08	1.8	4.41	0.20	3.03	101.42	15.79	80.88	85.73	90.58	64.22
24.06.08	0.4	2.23	0.20	2.81	111.14	15.52	76.67	81.42	84.51	61.47
25.06.08	0.2	2.10	0.20	3.56	120.56	20.32	73.64	78.48	78.63	60.13
26.06.08	0	4.32	0.20	5.43	90.07	14.38	69.80	74.63	72.73	57.71
27.06.08	0	3.84	0.20	6.06	106.68	16.17	60.74	65.75	53.85	54.78
28.06.08	0	4.59	0.17	4.60	144.44	19.80	55.17	60.88	45.82	49.38
29.06.08	0	3.49	0.18	5.47	126.52	16.61	52.38	56.23	39.80	52.64
30.06.08	5	2.84	0.17	5.13	146.62	19.67	48.96	51.87	35.89	51.53
01.07.08	0.2	2.03	0.14	3.99	-	-	-	-	-	-
02.07.08	0	2.92	0.15	4.08	153.02	29.52	44.98	47.19	33.24	48.11
03.07.08	0.4	2.51	0.15	3.91	136.38	24.56	40.33	40.49	29.20	47.41
04.07.08	0	2.40	0.17	3.71	-	-	-	-	-	-
05.07.08	0	1.65	0.17	4.52	-	-	-	-	-	-
06.07.08	0	3.56	0.19	4.92	144.15	21.05	30.16	28.17	17.58	42.73
07.07.08	0	2.63	0.17	5.47	140.17	32.00	30.34	27.43	17.30	45.11
08.07.08	0	2.15	0.16	4.14	143.39	25.23	23.87	20.65	10.48	39.53
09.07.08	0.4	6.91	0.15	4.58	-	-	-	-	-	-
10.07.08	0	10.22	0.17	2.72	169.40	38.30	21.12	18.46	3.75	38.25
11.07.08	2.2	6.77	0.16	2.25	-	-	-	-	-	-
12.07.08	22.4	3.42	0.10	3.14	-	-	-	-	-	-
13.07.08	14.4	5.80	0.13	5.46	139.01	49.73	17.78	12.95	4.91	36.49
14.07.08	0	3.26	0.15	6.06	157.62	37.35	17.36	13.58	3.69	34.42
15.07.08	0	1.54	0.17	5.63	165.82	25.42	14.46	11.03	1.07	30.61
16.07.08	0	1.62	0.22	8.23	159.70	23.15	13.51	10.26	0.71	28.84
17.07.08	0	3.04	0.19	8.03	165.85	24.09	13.06	9.46	0.54	28.96
18.07.08	0	4.36	0.17	8.36	193.93	36.82	12.55	9.17	0.78	27.48
19.07.08	0.8	2.05	0.15	5.66	-	-	-	-	-	-
20.07.08	5.2	3.01	0.15	6.02	167.23	27.79	10.74	7.36	0.27	24.80
21.07.08	1	2.42	0.14	6.51	-	-	-	-	-	-
22.07.08	0	2.71	0.18	8.92	152.93	31.74	9.56	5.94	0.40	23.29
23.07.08	0	3.80	0.21	10.15	188.21	37.52	9.01	5.90	0.00	21.55
24.07.08	0	3.09	0.21	6.54	199.66	38.06	8.71	5.53	0.03	21.18

continued

Table A-1: *continued*

	Precip.	Windsp.	Albedo	Temp.	Snow br.	Soil br.	SCA total	SCA west	SCA east	SCA slope
25.07.08	0	1.94	0.17	7.35	163.12	31.68	8.19	4.96	0.24	20.26
26.07.08	0	5.46	0.17	7.12	120.54	27.61	16.23	10.55	3.48	36.66
27.07.08	0	3.14	0.17	5.85	-	-	-	-	-	-
28.07.08	0	2.69	0.18	5.93	200.92	33.33	6.85	3.96	0.12	17.41
29.07.08	0.4	5.16	0.15	4.84	161.96	31.67	7.83	3.79	0.16	21.44
30.07.08	0	3.34	0.18	4.59	165.16	54.00	6.19	3.61	0.54	15.37
31.07.08	0	2.29	0.19	6.72	180.82	33.80	5.81	3.32	0.15	14.84
01.08.08	0	3.63	0.19	5.32	-	-	-	-	-	-
02.08.08	0	1.71	0.17	3.77	-	-	-	-	-	-
03.08.08	0	1.70	0.17	3.55	-	-	-	-	-	-
04.08.08	0	2.35	0.18	5.17	-	-	-	-	-	-
05.08.08	0	4.68	0.19	5.66	183.55	49.29	4.66	2.49	0.03	12.32
06.08.08	0	6.80	0.18	3.75	148.86	27.80	4.47	2.21	0.40	11.94
07.08.08	0	4.88	0.19	4.55	162.22	33.92	4.47	2.16	0.33	12.09
08.08.08	0.6	3.23	0.16	4.40	159.84	32.65	3.72	2.03	0.00	9.74
09.08.08	2.4	2.25	0.14	3.78	190.56	38.68	3.06	1.75	0.00	7.85
10.08.08	2	1.27	0.15	3.20	186.34	54.96	3.26	1.24	0.13	9.59
11.08.08	4.6	2.31	0.13	4.24	178.59	41.55	4.10	1.87	0.30	11.31

Table A-2: Snow depth measurements along a 16 m transect. Values are vertical cm.

distance (m)	24.07.08	26.07.08	28.07.08	30.07.08	01.08.08	03.08.08	05.08.08	07.08.08	09.08.08
0	42.5	0	0	0	0	0	0	0	0
1	52.5	37.5	20.5	3.5	0	0	0	0	0
2	65	45	27	23.5	8.5	10.5	0	0	0
3	74	50	42.5	32	21	16.5	0	0	0
4	71	60	55	32.5	24	10	0	0	0
5	74	65	42.5	27.5	30	32	0	0	0
6	76.5	75	57.5	29	24.5	21	0	0	0
7	75	66	37.5	32.5	20.5	10	0	0	0
8	77.5	57.5	45	32	25	21	5	2.5	0
9	85	65	57.5	43.5	35	33.5	21	2.5	0
10	112.5	71	62.5	51.5	41	35	20	11.5	10
11	115	78.5	65	51.5	46.5	36.5	33.5	25.5	21.5
12	87.5	96.5	86	61.5	45.5	51	32	30	17
13	97.5	90	69	56.5	45	35	22.5	25	0
14	77.5	77.5	57	57.5	42.5	35.5	24	15	8
15	42.5	55	40	38.5	27.5	0	0	0	0
16	20	35	0	0	0	0	0	0	0